Table 1. Intracellular histamine content of ES-derived MCs

Cells	Histamine content (pg/cell)
Experiment 1	
Es-MC (Day 40)	7.40 ± 0.49
Experiment 2	
Es-MC (Day 40)	7.58 ± 0.59
Experiment 3	
Es-MC (Day 50)	10.14 ± 1.82*
Human CB-MC (Day 70)	8.57 ± 1.22
Experiment 4	
Es-MC (Day 50)	11.32 ± 1.59*
Human CB-MC (Day 70)	9.44 ± 1.13

Five hundred ES-derived MCs (days 40 to 50) or human CB CD34+ cell-derived MCs (day 70) were lysed and the cell supernatant analyzed by an ELISA histamine assay kit. ($N = 4$)
*$p < 0.01$ as compared to human CB-MC (D70).

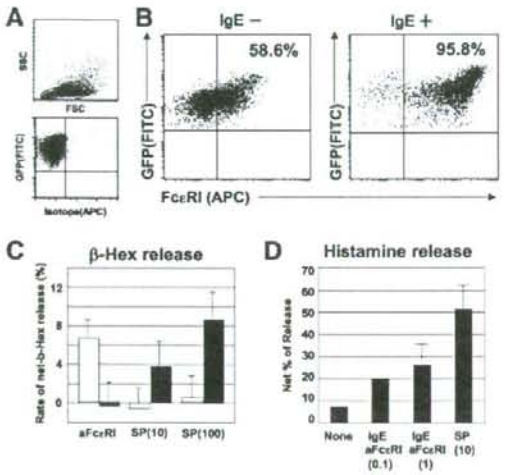

Figure 6. Primate embryonic stem (ES)-derived mast cells (MCs) functionally responded to IgE and substance P stimulation. **(A):** Distribution and negative control of primate ES-derived MCs by fluorescence-activated cell sorting analysis. The upper panel shows SSC and FSC distribution of day 40 cultured primate ES-derived MCs. The lower panel shows the isotope (allophycocyanin) negative staining. **(B):** When stimulated with 4 μg/ml IgE for 3 days, ES-derived MCs (day 40) upregulated expression of the FcεRI by up to 95.8%. **(C):** Net% β-Hex release was measured after stimulation of the FcεRI with mAb CRA-1 or exposure to 10 μM or 100 μM substance P. Human CB-derived MCs (white boxes) showed degranulation after CRA-1 treatment but not after the exposure to substance P, whereas ES-derived MCs (black boxes) responded to substance P in a dose-dependent manner. **(D):** Net% histamine release. To amplify the response, ES-derived MCs were pretreated with 1 μg/ml IgE overnight before stimulation with CRA-1. ES-derived MCs displayed a dose-dependent histamine release in response to CRA-1, as well as to 10 μM substance P. Abbreviations: APC, allophycocyanin; FSC, forward scatter; β-Hex, β-hexosaminidase; SP, substance P; SSC, side scatter.

at a low level (58.6%) but were highly upregulated (95.8%) after a 3-day exposure to 4 μg/ml IgE (Fig. 6A), similar to human and mouse MCs [19]. In addition, ES-derived MCs responded to stimulation with 10 μM substance P by releasing β-hexosaminidase (Fig. 6B) and histamine (Fig. 6C). To test responses to FcεRI stimulation, CRA-1, which specifically binds the α-chain of FcεRI was used. Human CB-derived MCs respond to CRA-1 treatment by degranulation, measured as β-hexosaminidase release, but did not respond to substance P (Fig. 6B), consistent with previous reports [3, 20]. In contrast to human CB-derived MCs, ES-derived MCs displayed dose-dependent degranulation in response to substance P stimulation. Because ES-derived MCs showed only marginal degranulation in direct exposure to CRA-1 in the β-hexosaminidase release assay (Fig. 6B), they were pretreated with 1 μg/ml IgE overnight to amplify the response to stimulation with CRA-1 in the histamine release assay. As a result, ES-derived MCs responded in a dose-dependent manner to CRA-1 as well as to substance P, as measured by histamine release (Fig. 6C). These results indicate that primate ES-derived MCs are functionally mature CT-MCs, not only because of the characteristic protease expression but also because of their ability to degranulate in response to pharmacological stimulation.

Discussion

In our present study, primate ES-derived progenitor cells, when specifically induced to undergo MC differentiation, generated mature MCs within only 3 weeks. These ES-derived MCs contained abundant, metachromatically stained granules and had high intracellular histamine content. They strongly expressed c-Kit and other MC-specific markers, and their surface antigen phenotype, c-Kit+/CD45+/CD31+/CD203+/HLA-DR−, was very similar to that of mature human MCs. Most interestingly, the ES-derived MCs possessed a chymase/tryptase double-positive phenotype and also stained positive for carboxypeptidase A and cathepsin G (data not shown). They expressed FcεRI on the surface, which was upregulated after IgE exposure. Moreover, these ES-derived MCs responded to stimulation with IgE and substance P by releasing histamine. These results indicate that primate ES-derived MCs have a CT-MC phenotype and are functionally similar to their human skin counterparts.

In fetal stages, murine MC precursors are highly concentrated in the yolk sac and fetal blood, suggesting there exists a strong early embryonic wave of MC development [8, 9]. However, because of the impossibility of conducting experimental manipulations on human embryos, little is known about human MC development during the embryonic and fetal stages. Full maturation of CT-MCs is thought to be achieved only after MC progenitors have migrated into the peripheral tissues. Although human CB-derived MCs give rise to tryptase/chymase double-positive MCs in long-term cultures, generally more than 10 weeks in vitro, they still cannot fully mimic the functions of CT-MCs in human skin, such as undergoing degranulation upon stimulation by substance P. Thus, the rapid maturation of primate ES-derived MCs in our present culture system suggests a unique embryonic pathway in primates for the early development of CT-MCs, which may be independent of M-MC development. We simultaneously cultured human CB CD34+ cells under the same culture conditions as in secondary MC cultures of ES-derived CS-like cells with an AGM-S1 feeder layer and found that they developed into MCs through a pathway in which they express tryptase (within 2 weeks) before they express chymase (more than 6 weeks) (data not shown). These data indicate that the primate ES-derived CT-MCs do not follow the same developmental pathway in vitro that has been described for MCs from human hematopoietic progenitors, as shown in MCs derived from CB or BM [21–22] in which tryptase is always expressed earlier than chymase. Rather, the development and maturation of MCs from ES-derived CS-like cells, a highly concentrated fraction of hematopoietic and hemangioblastic progenitors, may represent a unique route that is intrinsically

controlled during the early embryonic and fetal stages. Because CT-MCs such as those located in human skin possess a longer life span and higher potential for cell division than do M-MCs, CT-MC precursors may migrate to skin or other peripheral tissues at an early stage during fetal development.

A combination of cytokines, which included SCF, IL-6, and FL, was required to induce the optimal MC development from primate ES cells (Fig. 4C). This cytokine requirement was consistent with human MC development in vitro from CB. Among the cytokines we examined, FL seemed to expand the early hematopoietic pool but did not directly affect MC proliferation, because neither FL alone nor FL in combination with IL-6 could support MC growth, whereas FL+SCF stimulated formation of a few macrophages. FL was only effective in stimulating MC growth in combination with SCF+IL-6. On the other hand, stromal cell support of MC development has been well documented [23–25]. We found that proliferation and differentiation of ES-derived MCs decreased after 3 weeks in primary coculture if the AGM-S1 feeder layer became inadequate (Fig. 4A). ES-derived CS-like cells gave rise to only a few MCs when replated in culture dishes without AGM-S1 cells or on other stromal cells (data not shown). Notably, when day 40 ES-derived mature MCs (in secondary MC culture) were recultured either with AGM-S1 or without a stromal cell layer, the former cultures retained continuous growth while maintaining a chymase-dominant immunochemical phenotype, but the latter cultures gradually decreased in cell numbers and both tryptase and chymase expression was reduced (Fig. 4B; data not shown). These data suggest that AGM-S1 cells support both proliferation and maturation of the primate ES-derived CT-MCs, although the development of MCs from primate ES cells is not necessarily AGM-S1 cell-dependent.

Through our experiments, we could not confirm the specific progenitor type from which the ES-derived MCs arose. Nor could we determine what phenotype a committed ES-derived MC precursor possessed. Since a committed hematopoietic stem/progenitor cell has not yet been found in murine, human, or nonhuman primate ES cells, and because of the limited antibodies and genetic information specific for monkey ES cells and their progeny, pinpointing an ES-derived MC precursor has proven difficult. Although murine ES-derived functional MCs have been reported [26], because of considerable heterogeneity between rodent and human MCs, understanding of early human MC development using human and nonhuman primate ES cells is important. In this newly established in vitro culture system, large quantities of mature CT-MCs can be produced from primate ES cells in a relatively short time. Thus, our culture system will provide an excellent tool to further investigate the mechanisms that control early development of MCs in both human and nonhuman primates.

SUMMARY

We have illustrated a novel culture system for efficient production of CT-MCs with phenotypic and functional maturity from primate ES cells. The rapid maturation of ES-derived MCs suggests a unique embryonic pathway in primates for early development of CT-MCs, which may be independent from the developmental pathway of M-MCs. Our discovery should facilitate the further exploration of the unknown mechanisms that control early development of MCs in both human and nonhuman primates.

ACKNOWLEDGMENTS

We thank Dr. Y. Horiguchi (Osaka Redcross Hospital, Osaka, Japan) for conducting the electron microscopic observations. We also thank Prof. T. Nakano at Osaka University and Profs. H. Nakauchi, T. Kitamura, and S. Watanabe at the Institute of Medical Science, University of Tokyo, for constructive discussions. This work was supported in part by the Establishment of International COE for Integration of Transplantation Therapy and Regenerative Medicine and by Grants-in-Aid for Scientific Research from the Ministry of Education, Culture, Sports, Science and Technology of Japan. F.M. and N.K. contributed equally to this work.

DISCLOSURE OF POTENTIAL CONFLICTS OF INTEREST

The authors indicate no potential conflicts of interest.

REFERENCES

1 Kitamura Y, Shimada M, Hatanaka K et al. Development of mast cells from grafted bone marrow cells in irradiated mice. Nature 1977;268:442–443.
2 Irani AA, Schechter NM, Craig SS et al. Two types of human mast cells that have distinct neutral peotease compositions. Proc Natl Acad Sci U S A 1986;83:4464–4468.
3 Igarashi Y, Kurosawa M, Ishikawa O et al. Characteristics of histamine release from cultured human mast cells. Clin Exp Allergy 1996;26:597–602.
4 Toru H, Eguchi M, Matsumoto R et al. Interleukin-4 promotes the development of tryptase and chymase double-positive human mast cells accompanied by cell maturation. Blood 1998;91:187–195.
5 Kinoshita T, Sawai N, Hidaka E et al. Interleukin-6 directly modulates stem cell factor-dependent development of human mast cells derived from CD34(+) cord blood cells. Blood 1999;94:496–508.
6 Tam SY, Tsai M, Yamaguchi M et al. Expression of functional TrkA receptor tyrosine kinase in the HMC-1 human mast cell line and in human mast cells. Blood 1997;90:1807–1820.
7 Irani AM, Craig SS, DeBlois G et al. Deficiency of the tryptase-positive, chymase-negative mast cell type in gastrointestinal mucosa of patients with defective T lymphocyte function. J Immunol 1987;138:4381–4386.
8 Sonoda T, Hayashi C, Kitamura Y. Presence of mast cell precursors in the yolk sac of mice. Dev Biol 1983;97:89–94.
9 Rodewald HR, Dessing M, Dvorak AM et al. Identification of a committed precursor for the mast cell lineage. Science 1996;271:818–822.
10 Hanazono Y, Terao K, Ozawa K. Gene transfer into nonhuman primate hematopoietic stem cells: Implications for gene therapy. STEM CELLS 2001;19:12–23.
11 Suemori H, Tada T, Torii R et al. Establishment of embryonic stem cell lines from cynomolgus monkey blastocysts produced by IVF or ICSI. Dev Dyn 2001;222:273–279.
12 Umeda K, Heike T, Yoshimoto M et al. Development of primitive and definitive hematopoiesis from nonhuman primate embryonic stem cells in vitro. Development 2004;131:1869–1879.
13 Funiya M, Yasuchika K, Mizutani K et al. Electroporation of cynomolgus monkey embryonic stem cells. Genesis 2003;37:180–187.
14 Xu MJ, Tsuji K, Ueda T et al. Stimulation of mouse and human primitive hematopoiesis by murine embryonic aorta-gonad-mesonephros-derived stromal cell lines. Blood 1998;92:2032–2040.
15 Ma F, Wang D, Hanada S et al. Novel method for efficient production of multipotential hematopoietic progenitors from human embryonic stem cells. Int J Hematol 2007;85:371–379.
16 Ma F, Wada M, Yoshino H et al. Development of human lymphohematopoietic stem and progenitor cells defined by expression of CD34 and CD81. Blood 2001;97:3755–3762.
17 Nakahata T, Ogawa M. Hemopoietic colony-forming cells in umbilical cord blood with extensive capability to generate mono- and multipotential hemopoietic progenitors. J Clin Invest 1982;70:1324–1328.
18 Murakami M, Matsumoto R, Urade Y et al. c-kit ligand mediates increased expression of cytosolic phospholipase A2, prostaglandin endoperoxide synthase-1, and hematopoietic prostaglandin D2 synthase and

increased IgE-dependent prostaglandin D2 generation in immature mouse mast cells. J Biol Chem 1995;270:3239–3246.
19 Yamaguchi M, Sayama K, Yano K et al. IgE enhances Fc epsilon receptor I expression and IgE-dependent release of histamine and lipid mediators from human umbilical cord blood-derived mast cells: Synergistic effect of IL-4 and IgE on human mast cell Fc epsilon receptor I expression and mediator release. J Immunol 1999;162: 5455–5465.
20 Kambe N, Kambe M, Kochan JP et al. Human skin-derived mast cells can proliferate while retaining their characteristic functional and protease phenotypes. Blood 2001;97:2045–2052.
21 Saito H, Ebisawa M, Tachimoto H et al. Selective growth of human mast cells induced by Steel factor, IL-6, and prostaglandin E2 from cord blood mononuclear cells. J Immunol 1996;157:343–350.
22 Nakahata T, Tsuji K, Tanaka R et al. In: Kitamura Y, Yamamoto S, Galli SJ et al., eds. Biological and Molecular Aspects of Mast Cell and Basophil Differentiation and Function. New York: Raven Press, 1995: 13–24.
23 Furitsu T, Saito H, Dvorak AM et al. Development of human mast cells in vitro. Proc Natl Acad Sci U S A 1989;86:10039–10043.
24 Kirshenbaum AS, Kessler SW, Goff JP et al. Demonstration of the origin of the human mast cells from CD34+ bone marrow progenitor cells. J Immunol 1991;146:1410–1415.
25 Irani AA, Craig SS, Nilsson G et al. Characterization of human mast cells developed in vitro from fetal liver cells cocultured with murine 3T3 fibroblasts. Immunology 1992;77:136–143.
26 Tsai M, Wedemeyer J, Ganiatsas S et al. In vivo immunological function of mast cells derived from embryonic stem cells: An approach for the rapid analysis of even embryonic lethal mutations in adult mice in vivo. Proc Natl Acad Sci U S A 2000;97:9186–9190.

See www.StemCells.com for supplemental material available online.

Disease-associated *CIAS1* mutations induce monocyte death, revealing low-level mosaicism in mutation-negative cryopyrin-associated periodic syndrome patients

Megumu Saito,[1] Ryuta Nishikomori,[1] Naotomo Kambe,[2,3] Akihiro Fujisawa,[2] Hideaki Tanizaki,[2] Kyoko Takeichi,[4] Tomoyuki Imagawa,[5] Tomoko Iehara,[6] Hidetoshi Takada,[7] Tadashi Matsubayashi,[8] Hiroshi Tanaka,[9] Hisashi Kawashima,[10] Kiyoshi Kawakami,[11] Shinji Kagami,[12] Ikuo Okafuji,[1] Takakazu Yoshioka,[1] Souichi Adachi,[1] Toshio Heike,[1] Yoshiki Miyachi,[2] and Tatsutoshi Nakahata[1]

Departments of [1]Pediatrics and [2]Dermatology, Kyoto University Graduate School of Medicine, Kyoto; [3]Department of Dermatology, Chiba University Graduate School of Medicine, Chiba; [4]Department of Pediatrics, Ehime Prefectural Central Hospital, Matsuyama; [5]Department of Pediatrics, Yokohama City University School of Medicine, Yokohama; [6]Department of Pediatrics, Kyoto Prefectural University of Medicine, Graduate School of Medical Science, Kyoto; [7]Department of Pediatrics, Kyushu University Graduate School of Medicine, Fukuoka; [8]Department of Pediatrics, Seirei Hamamatsu Hospital, Hamamatsu; [9]Department of Pediatrics, School of Medicine, Hirosaki University, Hirosaki; [10]Department of Pediatrics, Tokyo Medical University, Tokyo; [11]Department of Pediatrics, Kagoshima City Hospital, Kagoshima; and [12]Department of Dermatology, University of Tokyo, Tokyo, Japan

Cryopyrin-associated periodic syndrome (CAPS) is a spectrum of systemic autoinflammatory disorders in which the majority of patients have mutations in the *cold-induced autoinflammatory syndrome (CIAS)1* gene. Despite having indistinguishable clinical features, some patients lack *CIAS1* mutations by conventional nucleotide sequencing. We recently reported a CAPS patient with mosaicism of mutant CIAS1, and raised the possibility that *CIAS1* mutations were overlooked in "mutation-negative" patients, due to a low frequency of mosaicism. To determine whether there were latent mutant cells in "mutation-negative" patients, we sought to identify mutation-associated biologic phenotypes of patients' monocytes. We found that lipopolysaccharide selectively induced necrosis-like cell death in monocytes bearing *CIAS1* mutations. Monocyte death correlated with *CIAS1* up-regulation, was dependent on cathepsin B, and was independent of caspase-1. Cell death was intrinsic to *CIAS1*-mutated monocytes, was not mediated by the inflammatory milieu, and was independent of disease severity or anti–IL-1 therapy. By collecting dying monocytes after lipopolysaccharide treatment, we succeeded in enriching *CIAS1*-mutant monocytes and identifying low-level *CIAS1*-mosaicism in 3 of 4 "mutation-negative" CAPS patients. Our findings reveal a novel effect of *CIAS1* mutations in promoting necrosis-like cell death, and demonstrate that *CIAS1* mosaicism plays an important role in mutation-negative CAPS patients. (Blood. 2008;111: 2132-2141)

Introduction

Cryopyrin-associated periodic syndrome (CAPS) is a spectrum of hereditary periodic fever disorders, and is associated with mutations in the *cold-induced autoinflammatory syndrome (CIAS)1* gene and its encoded protein, cryopyrin.[1] CAPS consists of 3 phenotypically overlapping but relatively distinct syndromes: familial cold autoinflammatory syndrome (FCAS), Muckle-Wells syndrome (MWS), and chronic infantile neurologic cutaneous and articular (CINCA) syndrome, also known as neonatal-onset multi-inflammatory disease. These syndromes are diagnosed mainly based upon clinical manifestations, among which an urticaria-like rash beginning in the neonatal or early infantile period is common. While FCAS and MWS are characterized by periodic attacks of urticarial rash, fever, and arthralgia, patients with CINCA syndrome, the most severe condition of CAPS, exhibit continuous disease activity, with fever, urticarial rash, arthropathy, chronic meningitis, papilledema, growth and mental retardation, and hearing loss.[1,2]

Recent genetic studies revealed that CAPS patients usually carry heterozygous mutations in the *CIAS1* coding region (mutation-positive patients[1-8]). Although they exhibit no recognizable differences in clinical symptoms or in their response to treatment, approximately half of CINCA syndrome patients lack detectable mutations in *CIAS1*, as assessed by conventional genomic sequencing (mutation-negative patients,[3-5,9-11]), indicating the existence of genetic heterogeneity among CAPS patients. Recently, we reported a patient with CINCA syndrome exhibiting mosaicism of a disease-associated mutation of *CIAS1*[12]. This case suggested that some mutation-negative CAPS patients might have mosaicism of the *CIAS1* mutation; however, the contribution of *CIAS1* mosaicism to disease is controversial. Aksentijevich et al claimed that *CIAS1* mosaicism is a rare event in mutation-negative patients, based on their analysis of 14 patients in which *CIAS1* mosaicism was not identified, even with careful bidirectional sequencing.[11,13,14]

Somatic mosaicism has been reported in a number of autosomal dominant monogenic disorders.[15-17] Diagnosis of mosaicism by conventional genomic sequencing using the dideoxy termination method is often difficult, because the overlapping chromatogram of the mutant is easily missed when the frequency of a mutant allele is less than 20% to 30%.[18] Heteroduplex-based methods[15,19] or subcloning-based analysis of mutant alleles enable one to detect

Submitted June 6, 2007; accepted November 29, 2007. Prepublished online as *Blood* First Edition paper, December 6, 2007; DOI 10.1182/blood-2007-06-094201.

The online version of this article contains a data supplement.

The publication costs of this article were defrayed in part by page charge payment. Therefore, and solely to indicate this fact, this article is hereby marked "advertisement" in accordance with 18 USC section 1734.

Table 1. Clinical profiles and *CIAS1* mutations identified in 11 patients with cryopyrin-associated periodic syndrome

Patient number	Diagnosis	Age, y*	Sex	Initial classification	Site of mutation	Biologics therapy	Central nervous system		Skin	Articular		Reference number
							Mental retardation	Meningitis	Urticarial rash†	Arthritis	Contracture	
1	CINCA	2	Female	Mutation-positive	N477K (1431C>A)	None	−	+	−	−	−	(28)
2	CINCA	3	Female	Mutation-positive	G755R (2263G>C)	Anakinra	−	+	−	+	−	(29)
3	CINCA	12	Male	Mutation-positive	M662T (1985T>C)	None	−	+	−	+	−	—
4‡	CINCA	12	Male	Mutation-positive	R260W (778C>T)	None	−	+	−	+	−	—
5	CINCA	13	Male	Mutation-positive	D303N (907G>A)	None	−	+	−	+	−	—
6	CINCA	14	Male	Mutation-positive	Y441H (1321C>T)	Tocilizumab	−	+	−	+	−	—
7	CINCA	15	Male	Mosaic	Y570C (1709A>G)	Anakinra§	−	+	−	+	−	(12)
8	CINCA	18	Female	Mutation-negative	L264F (790C>T)	None	−	+	−	−	−	(30)
9	CINCA	11	Male	Mutation-negative	G307S (919G>A)	None	−	−	−	+	+	—
10	MWS	27	Female	Mutation-negative	E567K (1699G>A)	None		Not assessed		+		(31)
11	CINCA	11	Male	Mutation-negative	Unknown	None	+	+	+	+	−	(32)

+ indicates present; −, not present; and —, not available

*Age at examination.

†Observed since neonatal period.

‡Father has the same heterozygous mutation of *CIAS1*.

§Administration of anakinra began during the study period.

such low-level mosaicism; however, these methods are resource-intensive, and cannot distinguish whether the detected mutation is disease-causing or simply a nonfunctional single nucleotide polymorphism (SNP). An alternative approach involves the isolation of mutant cells using functional analyses based on their characteristic biologic features, and then determining the DNA sequence of the isolated cells. In the current study, we set out to identify specific biologic features of *CIAS1*-mutant cells compared with nonmutated cells, in an effort to specifically isolate *CIAS1*-mutated cells from mutation-negative patients.

CIAS1 is expressed in peripheral blood polymorphonuclear cells (PBMCs), activated T cells, chondrocytes, and most prominently in monocytes.[4] The encoded protein, cryopyrin, belongs to a family of intracellular pattern recognition receptors, which are crucial in the control of immune responses, NF-κB activation, and cell death (reviewed in Ting and Davis[20] and Inohara et al[21]). Cryopyrin associates with caspase-1 and an adaptor protein called apoptosis-associated speck-like protein containing a caspase recruitment domain (CARD: ASC), forming a large protein complex called the inflammasome.[22-24] The inflammasome converts biologically inactive prointerleukin (proIL)-1β to active IL-1β, a potent proinflammatory cytokine, thereby causing an inflammatory response. It is speculated that mutant cryopyrin in CAPS patients activates the inflammasome constitutively in a ligand-independent manner. Indeed, enhanced production of IL-1β has been described in CAPS patients,[3,10,12,25] and is regarded as a primary cause of their inflammatory symptoms. Disease-associated *CIAS1* mutations induce ASC-dependent NF-κB activation in some systems,[12,22,26] and we recently reported that they also induce necrotic cell death in the human monocytic cell line THP-1, which is a novel function of *CIAS1*.[27]

In this study, we explored whether *CIAS1*-mutant cells have specific biologic features, using monocytes from mutation-positive patients, and found that *CIAS1*-mutant monocytes rapidly underwent necrosis-like cell death after treatment with lipopolysaccharide (LPS) to induce *CIAS1* expression. This unique phenotype of *CIAS1* mutant cells enabled us to differentiate *CIAS1*-mutated cells and nonmutated cells in 3 of 4 mutation-negative CAPS patients, and we were able to successfully demonstrate that these 3 patients had mutations of CIAS1 as latent mosaicism.

Methods

Patients

We recruited 11 Japanese CAPS patients, among whom 10 patients had clinically diagnosed CINCA syndrome, and 1 was diagnosed with MWS. All of the CINCA patients met previously described diagnostic criteria.[5,10] The MWS patient had recurrent episodes of inflammation that were not triggered by cold, progressive deafness, and amyloidosis. Written informed consents were obtained from the patients and their families, according to the protocol of the institutional review board of Kyoto University Hospital and in accordance with the Declaration of Helsinki. Details of patients are described in Table 1.

Reagents

Crude LPS (cLPS) from *Escherichia coli* O127:B8, muramyl dipeptide (MDP) and actinomycin D were purchased from Sigma-Aldrich (St Louis, MO). Pure LPS (pLPS), Pam3CSK, Poly I:C, recombinant flagellin, single-strand RNA (ss-RNA) and CpG DNA (type C, ODN M362) were from InvivoGen (San Diego, CA). Z-Tyr-Val-Ala-Asp(OMe)-CH_2F (YVAD-fmk), [L-3-*trans*-(propylcarbamoyl) oxirane-2-carbonyl]-L-isoleucyl-L-proline methyl ester (CA074-Me), and MG-132 were obtained from EMD (Darmstadt, Germany).

Culture of primary human cells

PBMCs were obtained from CAPS patients and healthy volunteers. $CD14^+$ monocytes and CD14 cells were purified by AutoMACS (Miltenyi Biotec, Gladbach, Germany), or sorted using a FACSVantage System (BD, Franklin Lakes, NJ). The purity of $CD14^+$ monocytes purified by AutoMACS and FACSVantage was more than 75% and 95%, respectively. PBMCs were cultured in RPMI1640 containing 10% fetal calf serum at a density of 10^6/mL with cLPS, MDP, or Toll-like receptor (TLR) ligands. In some experiments, PBMCs were preincubated for 30 minutes with YVAD-fmk (50 μM), CA074-Me (50 μM), or MG-132 (5 μM) before cLPS treatment.

Genetic analysis

Genomic DNA from PBMCs or whole blood was obtained as previously described.[12] To analyze the frequency of the *CIAS1*-mutant allele, exon 3 or the entire coding region of *CIAS1* was amplified using high fidelity DNA polymerase KOD plus (Toyobo, Osaka, Japan) and subcloned using a TOPO TA cloning kit (Invitrogen, Carlsbad, CA).[12] Genomic DNA and subclones were sequenced with an ABI 3100 sequencer (Applied Biosystems, Foster City, CA).

Real-time quantitative PCR

Total RNA was extracted from 1 to 2×10^5 monocytes using an RNeasy Mini kit (Qiagen, Venlo, Netherlands). After DNase I digestion (Invitrogen) and first-strand cDNA synthesis with Sensiscript RT (Qiagen), the products were subjected to real-time quantitative polymerase chain reaction (PCR) analysis of *CIAS1* and 18S rRNA (as an internal control) using an ABI PRISM 7900HT (Applied Biosystems). The following primers (200 nM) and probes (100 nM) were used: *CIAS1*, forward 5′-GAGCCTCAACAAACGCTACACA-3′, reverse 5′-CTTGCCGATGGCC-AGAAG-3′, probe 5′-FAM-CTGCGTCTCATCAAGGAGCACCGG-TAM-RA-3′; 18s rRNA, forward 5′-AGTCCCTGCCCTTTGTACACA-3′, reverse 5′-GATCCGAGGGCCTCACTAAAC-3′, probe 5′-FAM-CGCCCGTCGCTA-CTACCGATTGG-TAMRA-3′. Expression of *CIAS1* was normalized to 18S rRNA; expression is shown relative to *CIAS1* expression in the absence of LPS stimulation, which was set equal to one.

Allele-specific PCR

The PCR settings are described in Table S1 (available on the *Blood* website; see the Supplemental Materials link at the top of the online article) and were optimized to detect at least 0.6% of mutant alleles for each mutation. To make dilution series, patient DNA was diluted with DNA from an individual who was proved not to have latent mosaicism of *CIAS1* (confirmed by subcloning).

Flow cytometry

PBMCs were incubated with a FITC-conjugated anti–human CD14 mAb (BD), then sorted and analyzed using a FACScalibur System (BD). For intracellular IL-1β staining, cells were fixed, permeabilized, washed with Permfix and Cytoperm (BD), and incubated with a PE-conjugated anti–human IL-1β mAb (BD), at a concentration of 0.5 μg/mL. Cells were also incubated with propidium iodide (PI) or 7-aminoactinomycin D (7-AAD, purchased from BD) to identify nonviable cells. The expression of phosphatidylserine in the external layer of the plasma membrane was evaluated using PE-conjugated annexin-V (BD). In mutation-negative patients (patients 7-11), LPS-stimulated $CD14^-/PI^+$ cells and $CD14^-/PI^-$ cells were sorted using the FACSVantage System.

Cell viability assay

After incubation with or without cLPS, purified monocytes were centrifuged onto glass slides and were subjected to Giemsa staining. Cell viability was determined using a trypan blue exclusion assay.

Plasmids and cell lines

Expression plasmids for *CIAS1* and ASC in the pEF-BOS vector background have been described previously.[12] *CIAS1* mutants were generated using the QuikChange site-directed mutagenesis kit (Stratagene, La Jolla, CA).[12] The ability of each construct to induce NF-κB activation was assessed using a dual luciferase reporter assay in HEK293 cells as previously described.[12] cDNAs encoding carboxy-terminal green fluorescent protein (GFP)-tagged *CIAS1* and GFP-tagged mutants of *CIAS1* were subcloned into pcDNA/5TO (Invitrogen), before being introduced into human monocytic THP-1 cells using the Cell Line Nucleofector Kit V (Amaxa Biosystems, Cologne, Germany). Phorbol myristate acetate (10 ng/mL) was added to improve gene expression and reduce spontaneous cell death.[27] Four hours after the introduction of plasmids, cell death in GFP-positive THP-1 cells was measured by flow cytometry.

Statistical analysis

Data are represented as means plus or minus SD. Statistical analysis was performed using the Students *t* test. *P* less than .05 was considered to be statistically significant.

Results

Patient profile

To explore whether mutation-negative CAPS patients were misdiagnosed due to *CIAS1* mosaicism and the low frequency of the mutant allele, we recruited 11 Japanese CAPS patients. Clinical and genetic information for these patients is described in Table 1. Among them, 6 CINCA syndrome patients (patients 1-6) were confirmed as heterozygous for *CIAS1* mutation by ordinary genomic sequencing, and classified as mutation-positive patients, showing a frequency of the mutant allele of approximately 50% (data not shown). Patient 7 was previously diagnosed as a mosaic, in whom the frequency of the *CIAS1* mutant allele in whole blood was approximately 12%, reflecting that approximately 24% of blood cells carried the *CIAS1* mutation.[12] Three CINCA syndrome patients (patients 8-10) and 1 MWS patient (patient 11) had no evidence of overlapping peaks in their sequencing histograms, indicating that there were no point mutations in *CIAS1* that would correlate with amino acid substitutions, based on repeated bidirectional genomic sequencing. These patients were categorized as mutation-negative patients.

Spontaneous IL-1β production in monocytes at single-cell level

To find possible latent mosaicism in mutation-negative patients, we sought a method which enables mutant and normal cells from the reported mosaic patient to be distinguished at the single cell level. We investigated intracellular IL-1β staining as a candidate technique, because it is generally believed that enhanced production of IL-1β is the underlying molecular cause of CAPS.[10,33-35] To verify this, we first explored in vitro intracellular IL-1β production from CD14-positive peripheral monocytes by flow cytometry. Constitutive IL-1β up-regulation in monocytes was not detected in healthy controls ($n = 10$), but was observed in the confirmed mosaic patient (patient 7) before starting anakinra treatment (Figure 1). However, we were unable to resolve distinct high-producing ($IL\text{-}1\beta^{high}$) and low-producing ($IL\text{-}1\beta^{low}$) subpopulations of CD14-positive monocytes. In addition, while we sorted out relatively higher- and lower-intensity intracellular IL-1β fluorescence-staining populations, the frequency of the *CIAS1* mutant allele in each population was almost comparable (data not shown). Furthermore, when patient 7 was treated with anakinra, spontaneous IL-1β

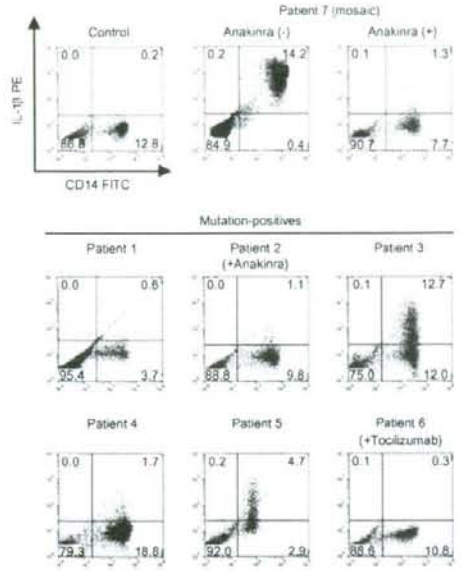

Figure 1. Intracellular IL-1β levels in PBMCs from CAPS patients. PBMCs from healthy controls (n = 10), mutation-positive patients (n = 6), or a mosaic patient (patient 7) were isolated and cultured in vitro for 24 hours. Flow cytometric analysis of CD14 expression and intracellular IL-1β levels was performed. The ratio of $CD14^{+}IL\text{-}1\beta^{high}$ monocytes (cells in the right upper quadrant) in healthy controls was 0.26% (± 0.43%; mean ± SD). Data from each of the indicated patients and a representative healthy control are shown. Numbers in each quadrant are the percentages of total cells.

up-regulation was canceled; therefore, the status of IL-1β production did not distinguish between monocytes with *CIAS1* mutations and those without. Two mutation-positive patients (patient 3 and 5) showed spontaneous up-regulation of intracellular IL-1β in monocytes upon culture of their PBMCs in vitro (Figure 1); this correlated with elevated IL-1β levels in culture supernatant (data not shown). The remaining mutation-positive patients, particularly those who received therapeutic biologics such as anakinra or the anti–IL-6R antibody tocilizumab (patients 2 and 6, respectively), did not show evidence of up-regulation of intracellular IL-1β. The status of intracellular IL-1β therefore seemed to be affected by various factors, such as the treatment applied. Two of the 4 mutation-negative patients (patients 10 and 11, data not shown) also exhibited an up-regulation of intracellular IL-1β. These results show that alterations in intracellular IL-1β levels were not helpful in finding latent mosaicism in mutation-negative patients.

Monocytes from CAPS patients rapidly undergo necrotic cell death when treated with LPS

We recently reported that overexpression of disease-associated mutants of *CIAS1* caused rapid necrosis-like cell death in a human monocytic cell line, THP-1.[27] As *CIAS1* is regulated by NF-κB, which is up-regulated by treatment with LPS,[16] we next verified whether LPS-induced up-regulation of CIAS1 could induce cell death in *CIAS1*-mutated monocytes. Quantitative mRNA analysis of *CIAS1* in mutation-positive patients and in healthy controls revealed that both cLPS and pLPS markedly enhanced *CIAS1* mRNA expression (Figure 2A). When stimulated with cLPS, the number of monocytes from all of the CAPS patients carrying a heterozygous *CIAS1* mutation (patients 1-6) decreased significantly, while in healthy controls, it did not (n = 10; Figure 2B,C). Although the magnitude of the decrease in monocyte number varied for each patient, this phenomenon was observed consistently, regardless of the disease severity, the level of spontaneous IL-1β production, or the therapeutic treatment regimen. Monocyte cell number was reduced to equal levels before and after anakinra treatment of patient 4, even though the clinical response to anakinra was excellent (data not shown). These results suggested that monocytes with *CIAS1* mutations undergo cell death when *CIAS1*

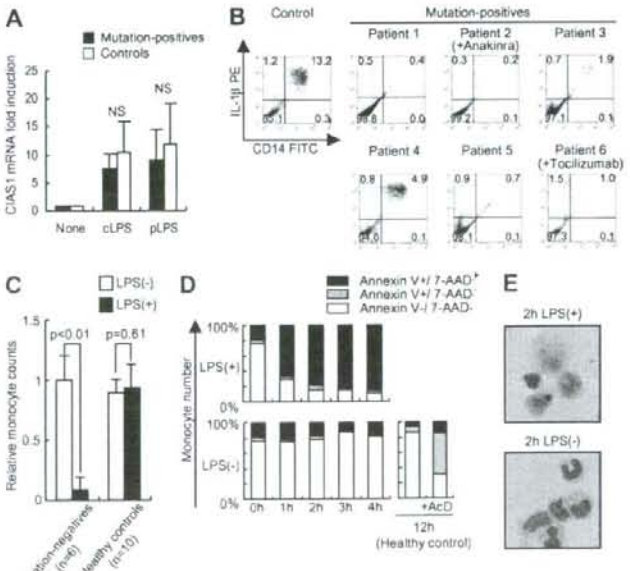

Figure 2. Monocytes from mutation-positive patients rapidly undergo cell death when treated with LPS. (A) Real-time quantitative reverse transcription (RT)-PCR analysis of *CIAS1* mRNA. Purified monocytes were incubated with cLPS (10 ng/mL) or pLPS (10 ng/mL) for 1 hour, and were then subjected to quantitative real-time RT-PCR analysis. Data were normalized to 18S rRNA expression, and represent the means (± SD) of 4 mutation-positive patients or 7 healthy controls. NS: statistically not significant. (B) Intracellular IL-1β staining of PBMCs from CAPS patients. PBMCs from mutation-positive patients (n = 6) or healthy controls (n = 10) were incubated with cLPS (10 ng/mL) for 24 hours. Flow cytometric analysis was performed as described for Figure 1. Representative results of each patient, or the control healthy patients, are shown. Numbers in each quadrant are the percentages of total cells. (C) Monocyte cell number decreases upon LPS stimulation. PBMCs were incubated with or without cLPS (10 ng/mL) for 24 hours, as described in Figure 1. Data represent the number of CD14-positive cells in 10 000 PBMCs, compared with the preincubation state, and represent the means (± SD) of the indicated number of patients. (D) PBMCs from mutation-positive patients were stained with FITC-conjugated anti-CD14, PE-conjugated anti-annexin V, and 7-AAD. Samples were analyzed by flow cytometry, gated to select CD14-positive cells, and then analyzed for cell viability. Data from normal PBMCs that were treated with actinomycin D (AcD, 1 μg/mL) for 12 hours were used as a positive control for apoptotis. Representative data from 5 mutation-positive patients are shown. (E) Giemsa staining of monocytes from mutation-positive patients incubated for 2 hours with or without cLPS. Cells were observed by inverted microscopy using an Olympus BX51 microscope (Olympus, Tokyo, Japan) equipped with a 40×/0.85 NA objective lens, an Olympus DP70 camera, and DP-controller version 1.1 software (Olympus). Data are representative of 3 mutation-positive patients.

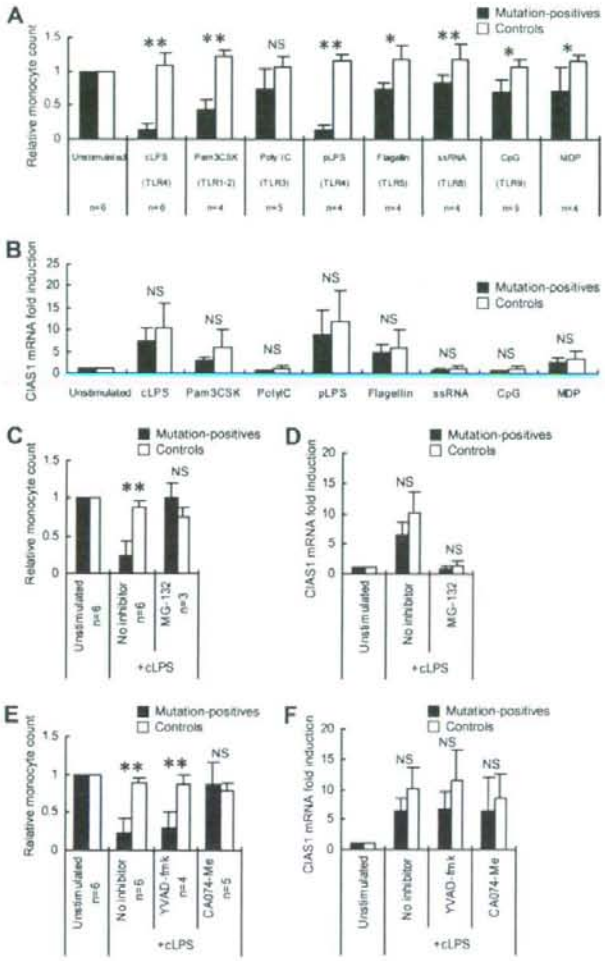

Figure 3. Effects of TLR ligands and various inhibitors on monocyte cell death. (A) PBMCs from mutation-positive patients or healthy controls were incubated for 24 hours with cLPS (10 ng/mL), MDP (5 μg/mL), Pam3CSK (10 μg/mL), Poly I:C (25 μg/mL), pLPS (10 ng/mL), recombinant flagellin (100 ng/mL), single-stranded RNA (ssRNA, 2 μg/mL), or CpG DNA (1 μM). The number of $CD14^+$ cells in 10 000 PBMCs was determined; the ratio of $CD14^+$ cells in stimulated PBMCs to those in unstimulated PBMCs is presented. Data represent the means (± SD) of the indicated number of patients or healthy controls ($n = 5$). (B) Real-time quantitative RT-PCR analysis of *CIAS1* mRNA. Purified monocytes were stimulated with TLR ligands or MDP, as described for (A), for 1 hour, and were then subjected to quantitative real-time RT-PCR analysis. Data were normalized to 18S rRNA expression, and represent the means (± SD) of 4 mutation-positive patients or 7 healthy controls. (C, E) PBMCs from the indicated number of mutation-positive patients or healthy controls ($n = 4$) were incubated with or without MG-132 (5 μM), YVAD-fmk (50 μM), or CA074-Me (50 μM) for 30 minutes before the addition of cLPS. The cells were then incubated with or without cLPS (10 ng/mL) for 4 hours. The ratio of $CD14^+$ and 7-AAD^- cells in 10 000 PBMCs relative to untreated cells is shown; data represent the means (± SD) (D, F) Real-time quantitative RT-PCR analysis of *CIAS1* mRNA. Purified monocytes were preincubated with the indicated inhibitors for 30 minutes, as described for (C and E), and were then stimulated with cLPS (10 ng/mL) for 1 hour. Thereafter, cells were collected and subjected to quantitative real-time RT-PCR analysis. Data were normalized to 18S rRNA expression. Values represent the means (± SD) of 4 mutation-positive patients or 7 healthy controls. **P* less than .05, ***P* less than .01, NS: not significant, compared with healthy controls by Student *t* test.

expression is induced by LPS. To confirm these results, flow cytometric analysis with PI or 7-AAD staining was performed. As shown in Figure 2D, CD14-positive monocytes from all of the heterozygous CAPS patients rapidly underwent cell death when treated with cLPS, while CD14-negative PBMCs did not (data not shown). When annexin-V staining was also examined, we found no evidence of a population of early apoptotic cells, defined as being annexin-V^+/7-AAD^- (lower right graph in Figure 2D); rather, cells became annexin-V/7-AAD double-positive directly, implying that they underwent necrosis, not typical apoptosis (Figure 2D). This result was comparable with previous observations using THP-1 cells.[27] Giemsa staining of cLPS-stimulated purified monocytes showed evidence of cellular debris from disrupted cells, but failed to detect typical apoptotic morphologic features, such as nuclear condensation or apoptotic bodies, even at early time points (1 or 2 hours) after cLPS stimulation (Figure 2E). Both cLPS and pLPS were equally effective in inducing monocyte death, excluding the possibility that unknown materials in cLPS were responsible for the effect (see Figure 3A). Thus, monocytes isolated from CAPS patients with *CIAS1* mutations rapidly underwent a type of cell death consistent with necrosis, rather than apoptosis, when treated with LPS.

Effect of TLR ligands on CIAS1 mutant monocytes

LPS is a ligand of TLR4,[37-39] which is constitutively expressed on monocytes.[40] Because monocytes express several types of TLR,[40] we investigated whether other TLR ligands were also able to induce cell death in *CIAS1*-mutant monocytes. As shown in Figure 3A, while several TLR ligands mildly or moderately decreased the number of monocytes from mutation-positive patients, none of them were as potent as LPS. MDP, a bacterial compound that was previously reported to be an activator of the cryopyrin inflammasome,[41] also mildly decreased monocyte number. Because some TLRs, such as TLR3 (receptor for poly I:C) and TLR9 (receptor for CpG DNA) are not typically expressed on monocytes,[40] modification of the cytokine milieu by other peripheral blood cells may have partly affected the fate of the mutant monocytes. Quantitative mRNA analysis of *CIAS1* in mutation-positive patients and in the healthy controls revealed that the effects of Pam3CSK and flagellin

on *CIAS1* expression were relatively mild, and the effects of poly I:C, single-stranded RNA, and CpG DNA were negligible (Figure 3B), consistent with the finding that LPS is the strongest inducer of cell death of *CIAS1* mutant monocytes. Furthermore, to inhibit the LPS-induced up-regulation of CIAS1 we pretreated monocytes with MG-132, a broadly effective proteasome inhibitor also known as a NF-κB inhibitor. The effect of LPS on monocyte death (Figure 3C) and *CIAS1* mRNA induction (Figure 3D) was completely abrogated. Although the possibility that MG-132 directly inhibits monocyte death cannot be excluded, these results suggested that the effect of LPS and other TLR ligands in inducing monocyte cell death is associated with their ability to enhance *CIAS1* expression.

LPS-induced death of monocytes with CIAS1 mutations is cathepsin B–dependent

Caspase-1 is a key downstream molecule of cryopyrin in IL-1β processing, and forms part of the inflammasome, along with cryopyrin and ASC.[23,42] We recently reported that the rapid necrosis of THP-1 cells induced by *CIAS1* disease-associated mutants was not mediated by a caspase-1-dependent pathway, but occurred in a lysosomal cathepsin B–dependent manner.[27] To explore the contribution of caspase-1 or cathepsin B in the LPS-induced cell death of *CIAS1*-mutant human primary monocytes, we pretreated PBMCs from mutation-positive patients with a caspase-1 inhibitor, YVAD-fmk, or a cathepsin B-specific inhibitor, CA074-Me (Figure 3E). YVAD-fmk was not effective in preventing monocyte cell death, even at a concentration which substantially suppressed LPS-induced IL-1β production (Figure S1). In contrast, CA074-Me effectively protected mutation-positive monocytes from LPS-induced cell death. Neither YVAD-fmk nor CA074-Me affected the up-regulation of *CIAS1* mRNA by LPS (Figure 3F), indicating that the effect of CA074-Me was not at the level of *CIAS1* expression, but that it inhibited a posttranscriptional pathway mediated by the mutant form of cryopyrin. Taken together, our findings implied a novel function of mutated *CIAS1* in inducing monocyte death in a cathepsin B-dependent, caspase-1–independent manner. The results also suggested that LPS-induced death of monocytes carrying disease-associated mutations of *CIAS1* is mediated by a similar mechanism to that reported for the cell death of human monocytic THP-1 cells induced by overexpression of mutated *CIAS1*.

Selective induction of cell death of CIAS1-mutated monocytes

To confirm that the cell death of *CIAS1* mutant monocytes was due to an intrinsic mechanism, rather than the result of modifications of the inflammatory milieu, we purified monocytes using magnetic sorting, stimulated them with LPS, and performed a trypan blue exclusion assay. We observed rapid cell death of purified monocytes upon cLPS stimulation, indicating that the monocytic death observed in the previous experiments was not mediated by other cells (Figure 4A). Giemsa staining of the purified monocytes also revealed features of necrosis-like cell death, as seen previously (Figure 2E).

Because patient 7 had mutant and nonmutant cells in the same milieu due to confirmed *CIAS1* mosaicism, we were interested in whether LPS-induced cell death was selective for monocytes carrying the *CIAS1* mutation. The percentage of CD14-positive monocytes from patient 7 tended to decrease slightly upon cLPS stimulation, but the cell survival profile was more similar to normal controls (Figure 4B). When the DNA of the monocytes from patient 7 was extracted and sequenced, there was an overlapping, small peak on the sequencing chromatogram in unstimulated PBMCs,

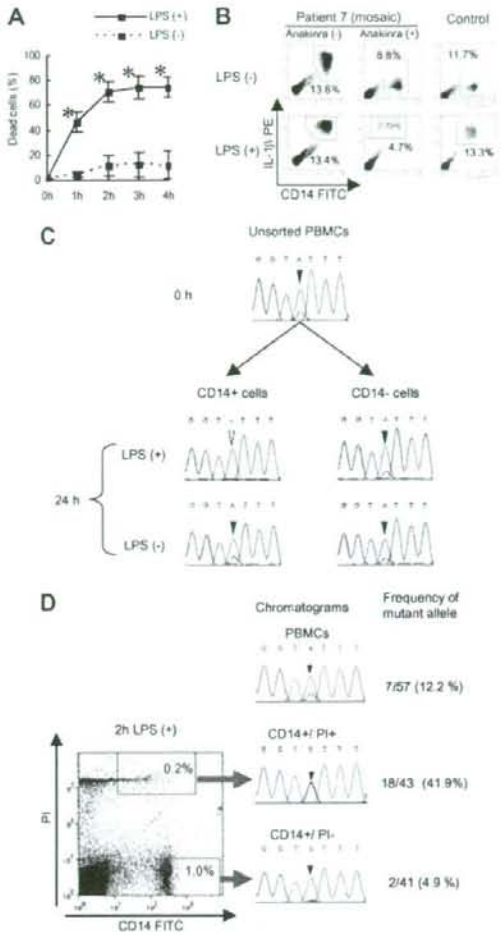

Figure 4. Selective elimination of mutated monocytes from mutation-positive and mosaic patients. (A) Trypan blue exclusion assay of purified monocytes. Purified monocytes were incubated with or without cLPS (10 ng/mL) and dead cells were counted. Values represent the means (± SD) of 3 mutation-positive patients. **P* less than .01 compared with LPS (-) counterparts. (B) Representative intracellular IL-1β staining of PBMCs from patient 7 or healthy controls after incubation with or without cLPS (10 ng/mL) for 24 hours. Numbers in each rectangle are the percentages of total cells. (C) PBMCs from patient 7 were cultured with or without cLPS (10 ng/mL) for 24 hours. CD14-positive and -negative cells were sorted, and DNA was extracted and sequenced for analysis of *CIAS1*. Chromatograms of the *CIAS1* gene at nucleotide position 1709 (black or white arrowhead) from each population of cells are shown. Note that the overlapping "G" peak (black arrowhead) disappeared from LPS-treated CD14-positive cells. The data are representative of 3 independent experiments. (D) *CIAS1*-mutated monocytes from a mosaic patient were enriched in the dying cell population. Left panel: flow cytometry data of PBMCs from patient 7 stimulated with cLPS for 2 hours. Right panel: chromatograms of the *CIAS1* gene at position 1709 (arrowhead), and frequency of the mutant allele as determined by subcloning from each population. The data are representative of 3 independent experiments.

indicating a mutation of the guanine (G) nucleotide at position 1709 (Figure 4C). In monocytes stimulated with cLPS, the histogram peak corresponding to the mutated G disappeared, while in unstimulated monocytes, or cLPS-stimulated, CD14-negative PBMCs, it did not (Figure 4C). These results suggested that cell death was induced selectively in *CIAS1*-mutated monocytes. When

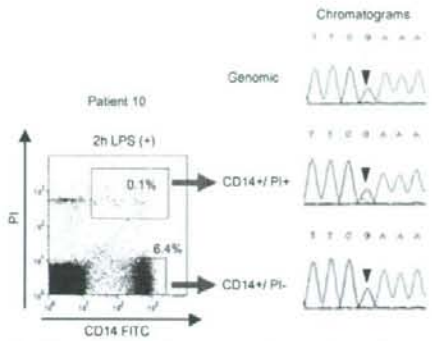

Figure 5. Enrichment of *CIAS1*-mutated monocytes from a *CIAS1* mutation-negative patient. Flow cytometry analysis of PBMCs from patient 10 stimulated with cLPS for 2 hours (left panel), and chromatograms of the *CIAS1* gene at position 1699 from each of the populations of cells (right panel). Numbers in each rectangle are the percentages of total cells.

we sorted CD14-positive/PI-negative cells and CD14-positive/PI-positive cells from cLPS-stimulated PBMCs from patient 7 (Figure 4D) and performed genomic DNA sequencing of each cell population. we found that *CIAS1*-mutated cells were enriched in the PI-positive population, and eliminated from the PI-negative population. Subcloning-based frequency analysis revealed successful enrichment of the mutant G allele, from a frequency of 12.2% in PBMCs to 41.9% in the PI-positive population of dying monocytes, correlating with an enrichment of mutated cells from approximately 25% to more than 80%. The frequency of the mutant allele in PI-negative monocytes that were not undergoing cell death significantly decreased, to 4.9%. These results suggested that cell death was induced exclusively in *CIAS1*-mutated monocytes, and not in normal cells, even though both cell types were exposed to the same extracellular milieu.

Identification of mosaicism in 3 of 4 CIAS1 mutation-negative CINCA patients

Based on the results from patient 7, we set out to identify *CIAS1* mosaicism in the remaining mutation-negative patients by enriching for PI^+, dying monocytes after cLPS stimulation. We stimulated PBMCs from patients 8-11 with cLPS, and while the decrease in monocyte cell number was comparable with normal controls (data not shown), we were able to sort dying (PI^+) from viable (PI^-) monocytes. Subsequent sequencing of the population of monocytes undergoing cell death revealed an overlapping peak on the sequencing chromatogram, indicating mosaicism, in 3 of 4 patients. The nucleotide substitutions were as follows (parentheses indicate the corresponding amino acid change): 790C > T (L264F) in patient 8; 919G > A (G307S) in patient 9; and 1699G > A (E567K) in patient 10 (Figure 5 and Figure S2). Overlapping peaks were not obvious in either chromatogram from unstimulated PBMCs or cLPS-stimulated, PI-negative monocytes. Subcloning analysis of genomic DNA from whole blood revealed that the mutant allele was enriched from 4.3% (2/47) to 19.4% (7/36) in patient 8, 4.3% (2/47) to 11.1% (3/27) in patient 9, and 6.5% (3/46) to 15.2% (7/46) in patient 10 (Table 2). The mutations and corresponding amino acid changes in patients 8, 9, and 10 have not been previously reported as either mutations or SNPs, and were not observed among 100 healthy Japanese donors (data not shown). We confirmed the existence of latent mosaicism in these patients by allele-specific PCR, which can detect mutant alleles at a frequency of 0.6% (Figure 6). We also analyzed 100 healthy controls to exclude the possibility of latent mosaicism among this population, and found no evidence of mutant *CIAS1* alleles (Figure 6 and data not shown). Thus, by selectively inducing cell death with LPS, we successfully diagnosed 3 CAPS patients who had been designated mutation-negative by conventional sequencing. Patient 11 had a phenotype that was marked by severe mental and developmental retardation. When we stimulated PBMCs from patient 11 with cLPS, there was very little cell death of monocytes, and we could not resolve overlapping peaks on the sequencing chromatogram of the population of dying monocytes (data not shown). We generated at least 54 subclones of the entire *CIAS1* coding region from patient 11, and confirmed that this individual did not carry any mutations, even as a mosaicism of *CIAS1*.

Table 2. Frequency of mutant alleles detected in mutation-negative patients

	Patient 8	Patient 9	Patient 10
Site of mutation	790C>T (L264F)	919G>A (G307S)	1699G>A (E567K)
Frequency of mutant allele			
Whole blood	2/47 (4.3%)	2/47 (4.3%)	3/46 (6.5%)
$CD14^+/PI^+$	7/36 (19.4%)	3/27 (11.1%)	7/46 (15.2%)
$CD14^+/PI^-$	2/46 (4.3%)	1/38 (2.6%)	3/48 (6.3%)

Disease-associated mutant CIAS1 induces cell death on THP-1 and spontaneous NF-κB activation

To evaluate whether the newly identified *CIAS1* mutations of this study were relevant to disease manifestation, we examined their ability to rapidly induce necrotic cell death when transiently expressed in human monocytic THP-1 cells (Figure 7A). The mutants identified in the mosaics (patients 7-10, Y570C, L264F,

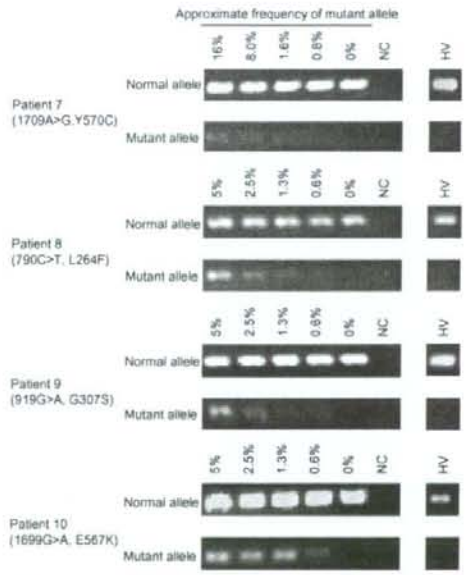

Figure 6. Allele-specific PCR for mutant alleles detected in mosaic patients. PCR was performed with mutant or normal allele-specific primers and the corresponding reverse primer (see Table S1). Dilution series were made by mixing patients' DNA and DNA from an individual who was proved not to have latent mosaicism of CIAS1. Representative results of mosaic patients and 100 healthy volunteers (HV) are shown. NC indicates negative control.

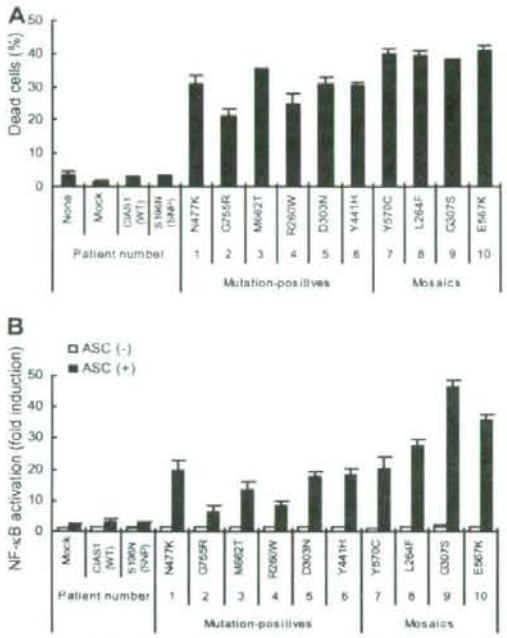

Figure 7. Effect of *CIAS1* mutation on the induction of cell death and ASC-dependent NF-κB activation. (A) 10^6 THP-1 cells were transfected with 0.5 μg of an expression vector for GFP-tagged *CIAS1* wild-type (WT), *CIAS1* SNP S196N, or one of the disease-associated mutants of *CIAS1* (R260W, L264F, D303N, G307S, Y441H, N477K, E567K, Y570C, M662T, and G755R), and incubated with PMA (10 ng/mL) for 4 hours. The percentage of dead cells (7-AAD-positive) among the population of GFP-positive cells is shown. Data represent the means (± SD) of triplicate determinations, and are representative of 3 independent experiments. (B) HEK293FT cells were transfected with 16 ng of an expression vector for *CIAS1*, or one of its mutants, in the presence or absence of 16 ng of an expression vector for ASC. The induction of NF-κB is shown as fold-change compared with cells that were transfected with a control vector without ASC (set equal to one). Values are the means (± SD) of triplicate determinations, and data are representative of 2 independent experiments.

G307S, and E567K) had more potent effects than those of the mutation-positive individuals. Transient coexpression of disease-associated *CIAS1* mutants and ASC in HEK293FT cells also caused enhanced NF-κB reporter activity, compared with the expression of wild-type *CIAS1*, or *CIAS1*-SNP S196N, a disease-unrelated *CIAS1* variant (Figure 7B).[12] Note that NF-κB activation induced by the mutants identified in mosaic patients was higher than that induced by the mutants identified in mutation-positive patients (patient 1-6; Figure 7B). These findings provided additional evidence that mutations of *CIAS1* that are found in both mutation-positive and mosaic patients are functional and related to the development of disease-related symptoms in CAPS patients.

Discussion

In the current study, we demonstrated that monocytes carrying disease-associated *CIAS1* mutations rapidly undergo cell death upon induction of *CIAS1* expression by LPS treatment. Selective induction of monocyte cell death was independent of the disease severity, level of IL-1β production, or therapeutic regimen. Subcloning and analysis of transient expression in cell lines indicated that the ability to induce cell death was specific to disease-associated mutations in *CIAS1*. Consequently, we were able to use this distinct biologic characteristic to enrich for monocytes carrying *CIAS1* mutations. We performed genetic analysis on 4 mutation-negative CAPS patients and found *CIAS1* mosaicism in 3 patients, while in the fourth we were able to exclude the presence of a mutation in the *CIAS1* coding region. These findings suggest that a majority of *CIAS1* mutation-negative patients have disease-associated mutations of *CIAS1* as a latent, low-level mosaicism.

Our results indicated that a small number of monocytes carrying *CIAS1* mutations are sufficient to evoke systemic inflammation in *CIAS1* mosaic patients. The question then arises of how such a small number of mutant cells cause the severe inflammatory responses observed in CAPS patients. As shown in Figure 1, we could not distinguish between *CIAS1*-mutated and nonmutated cells by intracellular IL-1β staining of PBMCs in patient 7 (mosaic patient); both mutated and nonmutated monocytes appeared to have similar levels of IL-1β. In patients who were treated with the IL-1 receptor antagonist anakinra, not only was IL-1β signaling blocked, but IL-1β production in peripheral blood monocytes was also dramatically reduced (Figure 1). This finding indicates that modification of the cytokine milieu due to the production of IL-1β by *CIAS1*-mutated cells, which possess constitutive IL-1β producing activity, may cause up-regulation of IL-1β in nonmutated monocytes, thereby leading to a systemic inflammatory condition. In support of this hypothesis, the addition of a neutralizing anti–IL-1β antibody to cultures of PBMCs from patient 7 reduced the levels of intracellular IL-1β, and addition of exogenous IL-1β to control, nonmutated monocytes induced an up-regulation in intracellular IL-1β (data not shown). In addition, we used transient transfection experiments to demonstrate that all of the *CIAS1* mosaic mutants (Y570C, L264F, G307S, and E567K) have the potential to induce higher NF-κB activity compared with wild-type *CIAS1* (Figure 7); thus, in patients in vivo, these mutations could be highly active, and sufficient to evoke severe systemic inflammation, even when present as a low-level mosaicism.

The clinical symptoms of mosaic patients appear to be milder than those of heterozygous patients. Patient 7 carried a *CIAS1*-Y570C mutation, which is one of the most common *CIAS1* mutations, and is associated with a very severe phenotype including mental retardation and epilepsy.[3,5,43] Patient 7 appeared to have milder symptoms than other reported heterozygous patients carrying the same mutation of *CIAS1*, showing neither mental retardation nor epilepsy, even at 15 years of age. Similarly, patient 8, who had the *CIAS1*-L264F mutation as mosaicism, exhibited a milder phenotype than patients with the heterozygous L264F mutation.[11] Although the *CIAS1*-G307S mutation in patient 9 has not yet been reported, the symptoms of the patient also seemed to be milder than that of a patient reported to have the G307V mutation.[44] The relatively mild phenotypes in mosaic patients, despite the relatively potent effects of their mutations on cellular activity (Figure 7), may be attributable to the lower dose of active mutation. Further study with more CAPS patients with CIAS1 mosaicism and more accurate measurements of mosaicism frequency by real-time PCR could provide clearer view of the correlation between the frequency of mutant allele and disease severity.

The mechanism of LPS-induced monocyte death that we observed remains to be elucidated. When monocytes are treated with LPS, *CIAS1* mRNA is induced immediately, and its encoded protein cryopyrin can be detected within 30 to 60 minutes of treatment.[36] One simple possibility is that the accumulation of LPS-induced mutant cryopyrin in the cytosol mediates necrosis. This is supported by our recent observation that overexpression of a

disease-associated mutant of *CIAS1* in THP-1 cells resulted in rapid necrosis-like cell death in a cathepsin B–dependent manner.[27] The caspase-1 inhibitor YVAD-fmk failed to inhibit LPS-induced monocyte cell death, while it effectively suppressed LPS-induced IL-1β production. Nigericin, a potassium ionophore, induces not only caspase-1–dependent IL-1β/IL-18 release but also rapid necrosis in LPS-primed THP-1 cells.[45] Interestingly, as we observed, the cathepsin B inhibitor CA074-Me inhibited the nigericin-induced necrosis while the caspase-1 inhibitor YVAD-cmk did not.[45] This indicates that a common pathway inducing cathepsin B-dependent necrosis in monocytes exists. Cross-talk between the LPS-TLR4 signaling pathway and the cryopyrin inflammasome to cause monocyte cell death is another possibility.

It was recently reported that the cytoplasmic receptor Ipaf recognizes bacterial flagellin, and induces rapid necrosis of *Salmonella*-infected macrophages.[46,47] It has been proposed that cryopyrin functions as a pattern-recognition receptor[48-50] that mediates inflammation; thus, it is possible that cryopyrin-induced rapid necrotic cell death and subsequent release of various cellular components facilitates local inflammation and prevents intracellular bacterial proliferation. Additional experiments are needed to clarify the mechanism of monocyte cell death observed in *CIAS1*-mutant cells in response to LPS.

While LPS-induced monocyte cell death seemed to be a specific property of *CIAS1* disease-associated mutant cells, the clinical and physiologic relevance of this biologic activity is unknown. The primary etiology of CAPS is considered to be excessive IL-1β production by constitutively activated inflammasomes. Although this hypothesis is supported by the fact that the autoinflammatory symptoms of the syndrome are successfully treated with IL-1β–targeted therapy,[10,29,33-35] it remains unclear whether the unique articular and cartilage manifestations of CAPS can also be attributed to IL-1β overproduction. Histologic analysis of the growth cartilage of CINCA syndrome patients revealed necrosis and disorganized proliferation of chondrocytes, and focal calcification, while infiltration of inflammatory cells was not described.[51] Feldmann et al speculated that the characteristic growth cartilage burst and epiphyseal overgrowth observed among CINCA patients might be due to dysregulated apoptosis of chondrocytes, which express a high amount of *CIAS1*.[4] One possibility is that certain stimuli, probably other than LPS, cause destructive necrosis of chondrocytes, rather than apoptosis, resulting in a loss of regularity of growth cartilage and subsequent bizarre joint destruction. We observed that LPS induces monocyte cell death independently of anti-IL-1β therapy status; thus, careful observation of anakinra-treated patients will provide a more precise understanding of the involvement of mutant *CIAS1*-mediated cell death in CAPS symptoms.

While the strategy we used in the current study was good at detecting single nucleotide substitutions, we cannot exclude the possibility that there were other types of genetic abnormalities present that were not detected, such as mis-splicing and noncoding region mutations. However, it is also possible that mosaicism, with an unequal distribution of mutant cells, is prominent in nonhematopoietic cells or tissues, such as the skin or central nervous system. An analysis of nonhematopoietic tissues may therefore be necessary before concluding that the *CIAS1* mutation is not responsible for the disease symptoms. Importantly, because diagnosis of CAPS is primarily based on clinical symptoms, a reassessment of the patients' histories and a physical re-evaluation is necessary before reestablishing the disease entity of *CIAS1*-unrelated patients.

In summary, we found that monocytes bearing mutations in *CIAS1* rapidly undergo necrosis-like cell death when treated with LPS, enabling us to diagnose *CIAS1* mutation-negative patients as *CIAS1* mosaic patients. Our investigation revealed that for a majority of CAPS patients without detectable *CIAS1* mutations by ordinary genomic sequencing, disease development may be attributable to low-level mosaicism. Not all *CIAS1* mutation-negative patients have *CIAS1* mosaicism, presenting the opportunity to uncover genes other than *CIAS1* as causative genes for CAPS. Our findings also raise the possibility that low-level mosaicism in other hereditary autoinflammatory syndromes may play a role in disease development, in the absence of detectable gene mutations.

Acknowledgments

We thank our CAPS patients and their parents for their participation. We thank Dr W. Strober (National Institutes of Health, Bethesda, MD) for critical reading of the manuscript and suggestions, and Dr S. Teramukai (Kyoto University, Kyoto, Japan) for advice on statistical analysis.

This study was supported in part by the Morinaga Hoshi-Kai; the Sapporo Bioscience Foundation; Ministry of Education, Science, Sports, and Culture; and the Ministry of Health, Labor, and Welfare, Japan.

Authorship

Contribution: M.S. performed research and wrote the paper. R.N. and N.K. designed the research, wrote the paper, and analyzed data. A.F. and H. Tanizaki performed research. K.T., T. Imagawa, T. Iehara, H. Takada, T.M., H. Tanaka, H.K., K.K., and S.K. treated the patients and analyzed data. I.O. and T.Y. performed research and discussed results. S.A. wrote the paper and discussed results. T.H., Y.M., and T.N designed the research.

Conflict-of-interest disclosure: The authors declare no competing financial interests.

Correspondence: Ryuta Nishikomori, MD, PhD, Department of Pediatrics, Kyoto University Graduate School of Medicine, 54 Kawahara-cho, Shogoin, Sakyo-ku, Kyoto 606-8507, Japan; e-mail: rnishiko@kuhp.kyoto-u.ac.jp.

References

1. Neven B, Prieur AM, Petty RE. Cryopyrin-associated periodic syndromes. In: Cassidy JT, Petty RE, Laxer RM, Lindsley CB, eds. Textbook of pediatric rheumatology 5th edition. Philadelphia, PA: Elsevier Saunders; 2005:671-675.
2. Prieur AM, Griscelli C, Lampert F et al. A chronic, infantile, neurologic, cutaneous and articular (CINCA) syndrome. A specific entity analysed in 30 patients. Scand J Rheumatol Suppl. 1987;66:57-68.
3. Aksentijevich I, Nowak M, Mallah M et al. De novo CIAS1 mutations, cytokine activation, and evidence for genetic heterogeneity in patients with neonatal-onset multisystem inflammatory disease (NOMID): a new member of the expanding family of pyrin-associated autoinflammatory diseases. Arthritis Rheum. 2002;46:3340-3348.
4. Feldmann J, Prieur AM, Quartier P et al. Chronic infantile neurological cutaneous and articular syndrome is caused by mutations in CIAS1, a gene highly expressed in polymorphonuclear cells and chondrocytes. Am J Hum Genet. 2002;71:198-203.
5. Neven B, Callebaut I, Prieur AM et al. Molecular basis of the spectral expression of CIAS1 mutations associated with phagocytic cell-mediated autoinflammatory disorders CINCA/NOMID, MWS, and FCU. Blood. 2004;103:2809-2815.
6. Hoffman HM, Mueller JL, Broide DH, Wanderer AA, Kolodner RD. Mutation of a new gene encoding a putative pyrin-like protein causes familial

cold autoinflammatory syndrome and Muckle-Wells syndrome. Nat Genet. 2001;29:301-305.

7. Aganna E, Martinon F, Hawkins PN et al. Association of mutations in the NALP3/CIAS1/PYPAF1 gene with a broad phenotype including recurrent fever, cold sensitivity, sensorineural deafness, and AA amyloidosis. Arthritis Rheum. 2002;46: 2445-2452.
8. Dodé C, Le Du N, Cuisset L et al. New mutations of CIAS1 that are responsible for Muckle-Wells syndrome and familial cold urticaria: a novel mutation underlies both syndromes. Am J Hum Genet. 2002;70:1498-1506.
9. Aróstegui JI, Aldea A, Modesto C et al. Clinical and genetic heterogeneity among Spanish patients with recurrent autoinflammatory syndromes associated with the CIAS1/PYPAF1/NALP3 gene. Arthritis Rheum. 2004;50:4045-4050.
10. Goldbach-Mansky R, Dailey NJ, Canna SW et al. Neonatal-onset multisystem inflammatory disease responsive to interleukin-1beta inhibition. N Engl J Med. 2006;355:581-592.
11. Aksentijevich I, D Putnam C, Remmers EF et al. The clinical continuum of cryopyrinopathies: novel CIAS1 mutations in North American patients and a new cryopyrin model. Arthritis Rheum. 2007;56:1273-1285.
12. Saito M, Fujisawa A, Nishikomori R et al. Somatic mosaicism of CIAS1 in a patient with chronic infantile neurologic, cutaneous, articular syndrome. Arthritis Rheum. 2005;52:3579-3585.
13. Aksentijevich I, Remmers EF, Goldbach-Mansky R, Reiff A, Kastner DL. Mutational analysis in neonatal-onset multisystem inflammatory disease: Comment on the articles by Frenkel et al and Saito et al. Arthritis Rheum. 2006;54:2703-2704.
14. Saito M, Fujisawa A, Nishikomori R et al. Reply. Arthritis Rheum. 2006;54:2704-2705.
15. Kwiatkowska J, Wigowska-Sowinska J, Napierala D, Slomski R, Kwiatkowski DJ. Mosaicism in tuberous sclerosis as a potential cause of the failure of molecular diagnosis. N Engl J Med. 1999; 340:703-707.
16. Kluwe L, Mautner V, Heinrich B et al. Molecular study of frequency of mosaicism in neurofibromatosis 2 patients with bilateral vestibular schwannomas. J Med Genet. 2003;40:109-114.
17. Youssoufian H, Pyeritz RE. Mechanisms and consequences of somatic mosaicism in humans. Nat Rev Genet. 2002;3:748-758.
18. Danielson PB, Kristinsson R, Shelton RJ, Laberge GS. Separating human DNA mixtures using denaturing high-performance liquid chromatography. Expert Rev Mol Diagn. 2005;5:53-63.
19. Emmerson P, Maynard J, Jones S, Butler R, Sampson JR, Cheadle JP. Characterizing mutations in samples with low-level mosaicism by collection and analysis of DHPLC fractionated heteroduplexes. Hum Mutat. 2003;21:112-115.
20. Ting JP, Davis BK. CATERPILLER: a novel gene family important in immunity, cell death, and diseases. Annu Rev Immunol. 2005;23:387-414.
21. Inohara N, Chamaillard M, McDonald C, Nunez G. NOD-LRR proteins: role in host-microbial interactions and inflammatory disease. Annu Rev Biochem. 2005;74:355-383.
22. Dowds TA, Masumoto J, Zhu L, Inohara N, Nunez G. Cryopyrin-induced interleukin 1beta secretion in monocytic cells: enhanced activity of disease-associated mutants and requirement for ASC. J Biol Chem. 2004;279:21924-21928.
23. Agostini L, Martinon F, Burns K, McDermott MF, Hawkins PN, Tschopp J. NALP3 forms an IL-1beta-processing inflammasome with increased activity in Muckle-Wells autoinflammatory disorder. Immunity. 2004;20:319-325.
24. Mariathasan S, Newton K, Monack DM et al. Differential activation of the inflammasome by caspase-1 adaptors ASC and Ipaf. Nature. 2004; 430:213-218.
25. Janssen R, Verhard E, Lankester A, Ten Cate R, van Dissel JT. Enhanced interleukin-1beta and interleukin-18 release in a patient with chronic infantile neurologic, cutaneous, articular syndrome. Arthritis Rheum. 2004;50:3329-3333.
26. Manji GA, Wang L, Geddes BJ et al. PYPAF1, a PYRIN-containing Apaf1-like protein that assembles with ASC and regulates activation of NF-kappa B. J Biol Chem. 2002;277:11570-11575.
27. Fujisawa A, Kambe N, Saito M et al. Disease-associated mutations in CIAS1 induce cathepsin B-dependent rapid cell death of human THP-1 monocytic cells. Blood. 2007;109:2903-2911.
28. Takada H, Kusuhara K, Nomura A et al. A novel CIAS1mutation in a Japanese patient with chronic infantile neurological cutaneous and articular syndrome. Eur J Pediatr. 2005;164:785-786.
29. Matsubayashi T, Sugiura H, Arai T, Oh-ishi T, Inamo Y. Anakinra therapy for CINCA syndrome with a novel mutation in exon 4 of the CIAS1 gene. Acta Paediatr. 2006;95:246-249.
30. Tanaka H, Waga S, Kakizaki Y, Sugimoto K, Nomura K, Yokoyama M. Chronic urticaria associated with aseptic meningitis: an atypical urticarial vasculitis? Acta Paediatr Jpn. 1997;39:64-68.
31. Kagami S, Saeki H, Kuwano Y, Imakado S, Tamaki K. A probable case of Muckle-Wells syndrome. J Dermatol. 2006;33:118-121.
32. Kawashima H, Sato A, Nisimata S et al. A case report of neonatal onset multisystemic inflammatory disease treated with continuous hemodiafiltration and steroid pulse therapy. Ther Apher Dial. 2007;11:232-234.
33. Hoffman HM, Rosengren S, Boyle DL et al. Prevention of cold-associated acute inflammation in familial cold autoinflammatory syndrome by interleukin-1 receptor antagonist. Lancet. 2004;364: 1779-1785.
34. Hawkins PN, Lachmann HJ, Aganna E, McDermott MF. Spectrum of clinical features in Muckle-Wells syndrome and response to anakinra. Arthritis Rheum. 2004;50:607-612.
35. Lovell DJ, Bowyer SL, Solinger AM. Interleukin-1 blockade by anakinra improves clinical symptoms in patients with neonatal-onset multisystem inflammatory disease. Arthritis Rheum. 2005;52: 1283-1286.
36. O'Connor W Jr., Harton JA, Zhu X, Linhoff MW, Ting JP. Cutting edge: CIAS1/cryopyrin/PYPAF1/NALP3/CATERPILLER 1.1 is an inducible inflammatory mediator with NF-kappa B suppressive properties. J Immunol. 2003;171:6329-6333.
37. Aderem A, Ulevitch RJ. Toll-like receptors in the induction of the innate immune response. Nature. 2000;406:782-787.
38. Poltorak A, He X, Smirnova I et al. Defective LPS signaling in C3H/HeJ and C57BL/10ScCr mice: mutations in Tlr4 gene. Science. 1998;282:2085-2088.
39. Qureshi ST, Lariviere L, Leveque G et al. Endotoxin-tolerant mice have mutations in Toll-like receptor 4 (Tlr4) J Exp Med. 1999;189:615-625.
40. Kadowaki N, Ho S, Antonenko S et al. Subsets of human dendritic cell precursors express different toll-like receptors and respond to different microbial antigens. J Exp Med. 2001;194:863-869.
41. Martinon F, Agostini L, Meylan E, Tschopp J. Identification of bacterial muramyl dipeptide as activator of the NALP3/cryopyrin inflammasome. Curr Biol. 2004;14:1929-1934.
42. Kuida K, Lippke JA, Ku G et al. Altered cytokine export and apoptosis in mice deficient in interleukin-1 beta converting enzyme. Science. 1995; 267:2000-2003.
43. Rösen-Wolff A, Quietzsch J, Schroder H, Lehmann R, Gahr M, Roesler J. Two German CINCA (NOMID) patients with different clinical severity and response to anti-inflammatory treatment. Eur J Haematol. 2003;71:215-219.
44. Matsubara T, Hasegawa M, Shiraishi M et al. A severe case of chronic infantile neurologic, cutaneous, articular syndrome treated with biologic agents. Arthritis Rheum. 2006;54:2314-2320.
45. Hentze H, Lin XY, Choi MS, Porter AG. Critical role for cathepsin B in mediating caspase-1-dependent interleukin-18 maturation and caspase-1-independent necrosis triggered by the microbial toxin nigericin. Cell Death Differ. 2003;10:956-968.
46. Franchi L, Amer A, Body-Malapel M et al. Cytosolic flagellin requires Ipaf for activation of caspase-1 and interleukin 1beta in salmonella-infected macrophages. Nat Immunol. 2006;7:576-582.
47. Miao EA, Alpuche-Aranda CM, Dors M et al. Cytoplasmic flagellin activates caspase-1 and secretion of interleukin 1beta via Ipaf. Nat Immunol. 2006;7:569-575.
48. Martinon F, Petrilli V, Mayor A, Tardivel A, Tschopp J. Gout-associated uric acid crystals activate the NALP3 inflammasome. Nature. 2006; 440:237-241.
49. Mariathasan S, Weiss DS, Newton K et al. Cryopyrin activates the inflammasome in response to toxins and ATP. Nature. 2006;440:228-232.
50. Kanneganti TD, Ozoren N, Body-Malapel M et al. Bacterial RNA and small antiviral compounds activate caspase-1 through cryopyrin/Nalp3. Nature. 2006;440:233-236.
51. De Cunto CL, Liberatore DI, San Roman JL, Goldberg JC, Morandi AA, Feldman G. Infantile-onset multisystem inflammatory disease: a differential diagnosis of systemic juvenile rheumatoid arthritis. J Pediatr. 1997;130:551-556.

EDITOR'S CHOICE

Use of multiplex PCR and real-time PCR to detect human herpes virus genome in ocular fluids of patients with uveitis

S Sugita,[1] N Shimizu,[2] K Watanabe,[2] M Mizukami,[3] T Morio,[3] Y Sugamoto,[1] M Mochizuki[1]

[1] Department of Ophthalmology & Visual Science, Medical Research Institute, Tokyo Medical and Dental University, Tokyo, Japan; [2] Department of Virology, Medical Research Institute, Tokyo Medical and Dental University, Tokyo, Japan; [3] Center for Cell Therapy, Tokyo Medical and Dental University, Tokyo, Japan

Correspondence to: Professor M Mochizuki, Department of Ophthalmology & Visual Science, Tokyo Medical and Dental University Graduate School of Medicine, 1-5-45 Yushima, Bunkyo-ku, Tokyo 113-8519, Japan; m.manabu.oph@tmd.ac.jp

Accepted 17 February 2008
Published Online First 11 April 2008

ABSTRACT

Aim: To measure the genomic DNA of human herpes viruses (HHV) in the ocular fluids and to analyse the clinical relevance of HHV in uveitis.

Methods: After informed consent was obtained, a total of 111 ocular fluid samples (68 aqueous humour and 43 vitreous fluid samples) were collected from 100 patients with uveitis. The samples were assayed for HHV-DNA (HHV1–8) by using two different polymerase chain reaction (PCR) assays, qualitative PCR (multiplex PCR) and quantitative PCR (real-time PCR).

Results: In all of the patients with acute retinal necrosis (n = 16) that were tested, either the HSV1 (n = 2), HSV2 (n = 3), or VZV (n = 11) genome was detected. In all patients, high copy numbers of the viral DNA were also noted, indicating the presence of viral replication. In another 10 patients with anterior uveitis with iris atrophy, the VZV genome was detected. When using multiplex PCR, EBV-DNA was detected in 19 of 111 samples (17%). However, real-time PCR analysis of EBV-DNA indicated that there were only six of the 19 samples that had significantly high copy numbers. The cytomegalovirus (CMV) genome was detected in three patients with anterior uveitis of immunocompetent patients and in one immunocompromised CMV retinitis patient. In addition, one patient with severe unilateral panuveitis had a high copy number of HHV6-DNA. There was no HHV7- or HHV8-DNA detected in any of the samples.

Conclusions: A qualitative multiplex PCR is useful in the screening of viral infections. However, the clinical relevance of the virus infection needs to be evaluated by quantitative real-time PCR.

Human herpes virus (HHV) affects various ocular tissues and is known to cause anterior and/or posterior uveitis, which is characterised by mutton-fat keratic precipitates (KPs), ocular hypertension, iris atrophy, vitreous opacity, and necrotic retinitis. Using polymerase chain reaction (PCR), previous studies have demonstrated the presence of genomic DNA for HHV in the aqueous humour and vitreous fluids in patients with herpetic uveitis, including herpetic keratouveitis, herpes zoster ophthalmicus, zoster sine herpete, acute retinal necrosis, and cytomegalovirus retinitis.[1–7] With recent advances in molecular biology, use of real-time PCR now makes it possible for quantitative measurements of the viral load associated with herpes virus diseases in the eye.[8 9] In addition, multiplex qualitative PCR has the advantage of combining several different primer pairs in the same amplification reaction with the net result of producing different specific virus-amplicons in ocular infectious diseases.[7] Therefore, multiplex PCR can be used to detect the presence of viruses within samples.

In this study, we collected ocular samples from various uveitis patients and then tried to detect the HHV genome when using combinations of two PCR systems: (1) multiplex qualitative PCR and (2) real-time quantitative PCR.

MATERIAL AND METHODS

Subjects

Samples of aqueous humour (n = 68) and vitreous fluid (n = 43) were collected from 100 patients with uveitis and ocular lymphoma. Underlying pathology comprised herpetic keratouveitis (n = 7), herpetic anterior uveitis/iridocyclitis (n = 16), acute retinal necrosis (ARN; n = 16), cytomegalovirus (CMV) retinitis (n = 1), human T lymphotropic virus type 1 (HTLV-1) uveitis (n = 1), ocular toxoplasmosis (n = 2), scleritis (n = 3), ocular sarcoidosis (n = 7), Vogt–Koyanagi–Harada (VKH) disease (n = 2), Behçet disease (n = 2), idiopathic uveitis (n = 26) and intraocular lymphoma (n = 12). At the time of sampling, uveitis patients displayed active intraocular inflammation.

An aliquot of 0.1 ml of the aqueous humour was aspirated with a 30 G needle. In patients with uveitis who were undergoing vitreous surgery, non-diluted vitreous fluid samples were collected from the patients during surgery (diagnostic pars-plana vitrectomy). The samples used in this study were collected between 1999 and 2007.

Polymerase chain reaction

Genomic DNA of HHV in the aqueous humour and vitreous fluids was measured through the use of two independent PCR assays: (1) a qualitative multiplex PCR and (2) a quantitative real-time PCR. The result analysis for the PCR is shown in fig 1.

DNA was extracted from samples using an E21 virus minikit (Qiagen, Valencia, CA) installed on a Robotic workstation for automated purification of nucleic acids (BioRobot E21, Qiagen). The multiplex PCR was designed to qualitatively measure genomic DNA of eight human herpes viruses, that is, herpes simplex virus type 1 (HSV-1), type 2 (HSV-2), Varicella-zoster virus (VZV), Epstein–Barr virus (EBV), cytomegalovirus (CMV), human herpes virus type 6 (HHV6), type 7 (HHV7) and type 8 (HHV8). The PCR was performed using a

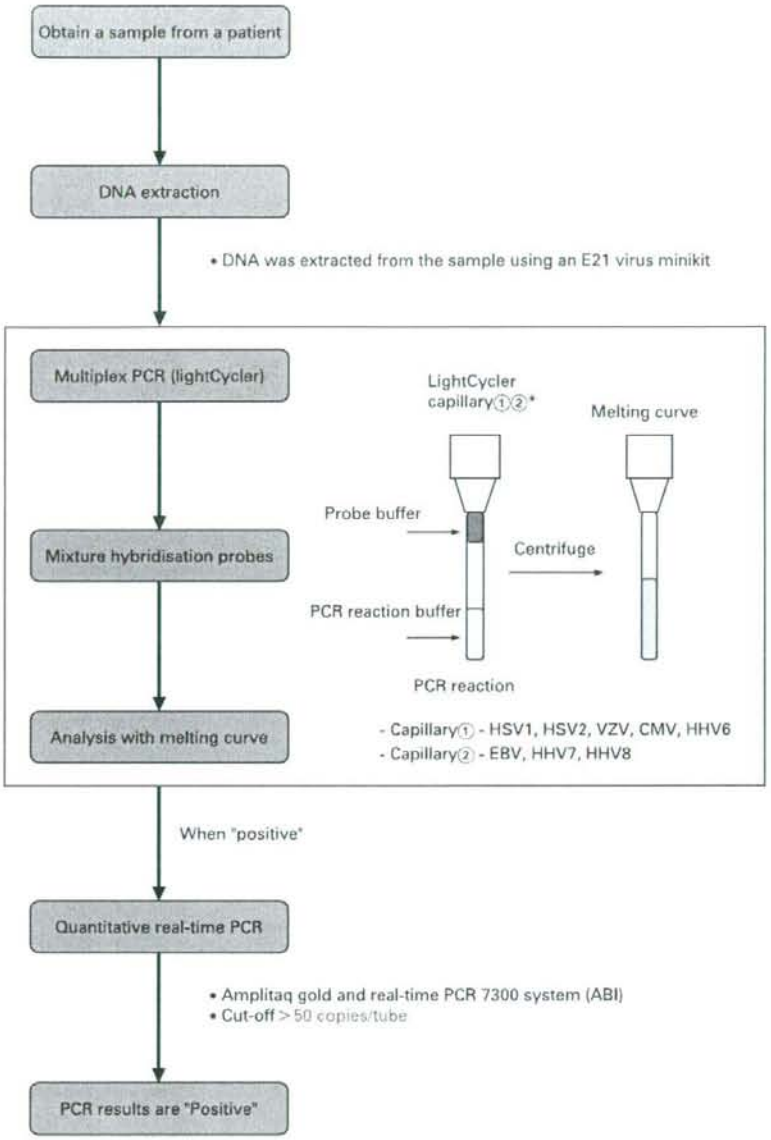

Figure 1 Use of multiplex PCR and real-time PCR for the analysis of human herpes virus family genomic DNA in ocular fluids of patients with uveitis. We performed independent PCR methods to detect herpes viruses, using both a qualitative multiplex PCR and a quantitative real-time PCR. After DNA extraction from each of the samples, multiplex PCR was performed to screen from HHV1 to HHV8 using two LightCycler capillaries. When a "positive" result was observed, real-time PCR was performed to measure the viral load. When more than 50 copies/tube (5×10^3/ml) were observed, the value was considered to be significant. CMV, cytomegalovirus; EBV, Epstein–Barr virus; HHV, human herpes virus; HSV, herpes simplex virus; VZV, Varicella-zoster virus.

LightCycler (Roche, Switzerland). Primers and probes of HHV1–8 and the PCR conditions have been described previously.[8] Specific primers for the virus were used with Accuprime Taq (Invitrogen, Carlsbad, CA). Products were subjected to 40 cycles of PCR amplification. Hybridisation probes were then mixed with the PCR products. Subsequently, real-time PCR was performed only for the human herpes virus, with the genomic DNA detected by multiplex PCR (fig 1). The real-time PCR was performed using Amplitaq Gold and the Real-Time PCR 7300 system (ABI, Foster City, CA). The sequence of the HHV1–8 primers and probes are shown in table 1. The primers of the viruses and the PCR conditions have been described in previous reports.[9 10] Our research group has also previously reported the primers of the sequences for VZV.[11] All of the products obtained were subjected to 45 cycles of PCR amplification. The value of viral copy number in the sample was considered to be significant, when more than 50 copies/tube (5×10^3/ml) were observed.

RESULTS

Our initial PCR results indicated HHV positivity in the ocular fluids of uveitis patients. As shown in table 2, multiplex PCR detected seven patients with HSV1-DNA while real-time PCR found that all seven of these patients also had a high HSV1 viral load. In addition, HSV2-DNA was detected in three patients, with all of these patients having a high viral load. In 29 patients,

Table 1 Sequence for primers and probes in human herpes viruses (HHV) using real-time PCR

Herpes virus	Sequence for primers and probes	Amplification
HSV1 and 2	HSV-F: CGCATCAAGACCACCTCCTC	gB
	HSV-R: GCTCGCACCACGCGA	
	HSV1-P: JOE-TGGCAACGCGGCCCAAC-TAMRA	
	HSV2-P: FAM-CGGCGATGCGCCCCAG-TAMRA	
VZV	VZV-F: AACTTTTACATCCAGCCTGGCG	ORF29
	VZV-R: GAAAACCCAAACCGTTCTCGAG	
	VZV-P: FAM-TGTCTTTCACGGAGGCAAACACGT-TAMRA	
EBV	EBV-F: CGGAAGCCCTCTGGACTTC	BALF5
	EBV-R: CCCTGTTTATCCGATGGAATG	
	EBV-P: FAM-TGTACACGCACGAGAAATGCGCC-TAMRA	
CMV	CMV-F: CATGAAGGTCTTTGCCCAGTAC	IE-1
	CMV-R: GGCCAAAGTGTAGGCTACAATAG	
	CMV-P: FAM-TGGCCCGTAGGTCATCCACACTAGG-TAMRA	
HHV6	HHV6-F: GACAATCACATGCCTGGATAATG	U65-U66
	HHV6-R: TGTAAGCGTGTGGTAATGTACTAA	
	HHV6-P: FAM-AGCAGCTGGCGAAAAGTGCTGTGC-TAMRA	
HHV7	HHV7-F: CGGAAGTCACTGGAGTAATGACAA	U37
	HHV7-R: CCAATCCTTCCGAAACCGAT	
	HHV7-P: FAM-CTCGCAGATTGCTTGTTGGCCATG-TAMRA	
HHV8	HHV8-F: CCTCTGGTCCCCATTCATTG	ORF65
	HHV8-R: CGTTTCCGTCGTGGATGAG	
	HHV8-P: FAM-CCGGCGTCAGACATTCTCACAACC-TAMRA	

The real-time herpes simplex virus (HSV) PCR is a multiplexing PCR that can detect both HSV1 and HSV2 DNA in the same reaction. The optimised gB primer pairs amplify both HSV1 and 2 with equal efficiency, with the two type-specific probes labelled with different fluorescent dyes. HSV1 probe is labelled with JOE at the 5'-end and with TAMRA at the 3'-end. HSV2 probe is labelled with FAM at the 5'-end and with TAMRA at the 3'-end.
CMV, cytomegalovirus; EBV, Epstein-Barr virus; VZV, Varicella-zoster virus.

VZV-DNA was detected, but only 21 patients (72%) had a high viral load. EBV was detected in 19 patients, but only six out of the 19 cases were positive (32%). CMV-DNA was detected in six patients, with four out of the six cases (67%) found to be positive by the real-time PCR. HHV6-DNA was detected in only one patient by both of the PCR methods. There were no patients for which HHV7 and HHV8 were detected. Overall, there were 65 multiplex PCR positive patients and 42 real-time PCR positive patients (table 2). Clinically, we decided that only if HHV-DNA could be detected in a sample (aqueous humour and/or vitreous) by both PCR methods would the patient then be considered to be positive. If a patient was found to be positive by only one of the PCR methods, for example, positive by multiplex qualitative PCR and negative (<50 copies/tube) by real-time quantitative PCR, we did not take this as PCR-positive (fig 1).

Table 2 Human herpes virus-PCR positivity in ocular fluids of 100 patients with uveitis

Herpes virus	Multiplex PCR	Real-time PCR
HSV1	7/100 (7%)	7/7 (100%)
HSV2	3/100 (3%)	3/3 (100%)
VZV	29/100 (29%)	21/29 (72%)
EBV	19/100 (19%)	6/19 (32%)
CMV	6/100 (6%)	4/6 (67%)
HHV6	1/100 (1%)	1/1 (100%)
HHV7	0/100 (0%)	–
HHV8	0/100 (0%)	–
Total	65/100 (65%)	42/65 (65%)

Qualitative multiplex PCR was performed in order to screen for and detect human herpes virus (HHV) genomic DNA, HHV1-HHV8. When the genomic DNA was detected by the multiplex PCR (n = 65), real-time PCR was then performed only for the HHV.
CMV, cytomegalovirus; EBV, Epstein-Barr virus; HSV, herpes simplex virus; VZV, Varicella-zoster virus.

Subsequently, we analysed the results for each the viruses, from HHV1 to HHV8. The summary of the results is shown in table 3. HSV1 was detected in two cases of keratouveitis, and in three cases of anterior uveitis. These patients had mutton-fat KPs, ocular hypertension and anterior chamber cells. HSV1 was also detected in two cases of acute retinal necrosis (ARN). HSV2 was detected in three cases of ARN. VZV was detected in 10 cases of herpetic anterior uveitis and in 11 cases of ARN. During the time after the initial onset of anterior uveitis, iris atrophy developed in these patients. Higher viral load in the aqueous humour was well correlated with tissue damage, such as iris atrophy.[14] In addition, as we have reported previously, real-time PCR of the ocular fluids from ARN patients (n = 16) indicated high viral loads of VZV (n = 11, 69%), HSV1 (n = 2, 12%), and HSV2 (n = 3, 19%).[8]

EBV was detected in only one case of idiopathic uveitis. This patient had acute anterior uveitis with hypopyon and was HLA-B27 negative. Therefore, as previously reported, we diagnosed EBV-related acute anterior uveitis.[15] EBV was also detected in two cases of VZV-associated anterior uveitis and in two cases of VZV-ARN. This suggests that these patients have a high copy number of VZV, as well as EBV in their ocular fluids. EBV was also detected in one case of ocular B-cell lymphoma.

CMV was detected in a case of cytomegalovirus retinitis and in three cases of CMV-associated anterior uveitis. Representative results from the multiplex qualitative PCR can be seen in fig 2. CMV-DNA was detected in the aqueous humour, and quantitative real-time PCR revealed there were 2.5×10^{5} copies/mL of CMV-DNA in the specimen. As we previously reported, in the affected eye there were whitish small-size mutton-fat KPs along with mild inflammation in the anterior chamber.[16] During the 8 years this particular patient was followed, he had been considered to have a case of Posner–Schlossman syndrome. This patient had no retinitis, and additionally he was not found to be immunocompromised.

Br J Ophthalmol 2008;**92**:928–932. doi:10.1136/bjo.2007.133967

Table 3 PCR results for each herpes virus genome in patients with uveitis

Herpes virus	Clinical diagnosis	PCR-positive*/total no of patients
HSV1	Herpetic keratouveitis	2/7†
	Herpetic anterior uveitis	3/16
	Acute retinal necrosis	2/16
	Others	0/61
HSV2	Acute retinal necrosis	3/16
	Others	0/84
VZV	Herpetic anterior uveitis	10/16
	Acute retinal necrosis	11/16
	Others	0/68
EBV	Idiopathic uveitis	1/26
	Herpetic anterior uveitis (VZV)	2/16
	Acute retinal necrosis (VZV)	2/16
	Intraocular lymphoma	1/12
	Others	0/30
CMV	Herpetic anterior uveitis	3/16
	Cytomegalovirus retinitis	1/1
	Others	0/83
HHV6	Idiopathic uveitis	1/26
	Others	0/74
HHV7	–	0/100
HHV8	–	0/100

*Detection of HHV-DNA by both multiplex PCR and real-time PCR.
†In the seven patients with keratouveitis, our PCR system detected HSV1-DNA in two patients.
CMV, cytomegalovirus; EBV, Epstein–Barr virus; HHV, human herpes virus; HSV, herpes simplex virus; VZV, Varicella-zoster virus.

A high copy number of HHV6-DNA was detected in only one patient with severe unilateral panuveitis. In this patient, multiple retinal exudates, vitreous opacity, along with a whitish mass lesion were observed in the affected eye. We reported this case as HHV6-associated panuveitis.[17] In the current study, HHV7- or HHV8-DNA was not detected in any of the patients (table 3).

DISCUSSION

Human herpes viruses (HHV) can widely affect the eye and be expressed in ocular tissues or excreted in ocular fluids. Previously, the diagnosis of intraocular HHV infection was made by measuring local production of specific anti-virus antibodies—for example, using the Goldmann–Witmer coefficient. Recently, diagnosis has also been performed through the detection of the virus genome by PCR. Cell-free herpes virus DNA has been detected in the aqueous humour and vitreous fluids of patients with uveitis.[1 2] In the current study, we showed that intraocular HHV-DNA was detectable over a wide range of HHV-associated uveitis when analysis was performed using the two PCR methods. Thus, the current PCR system may be a valuable tool in the diagnosis of infectious uveitis. In addition, with the use of these examinations, this allows non-herpetic uveitis patients to be excluded.

When faced with a clinical situation that suggests a differential diagnosis of HHV1–8, the multiplex PCR assay can provide a rapid and reliable diagnosis, even when only small sample amounts are available for examination in the ocular microbiology laboratory. The majority of the viruses associated with eye diseases are related to the herpes virus group. Therefore, the last decade has seen several studies concluding that herpes virus PCR-based laboratory investigations are valuable tools in the diagnosis of viral diseases of the eye. The advantages of developing the multiplex PCR assay are obvious,

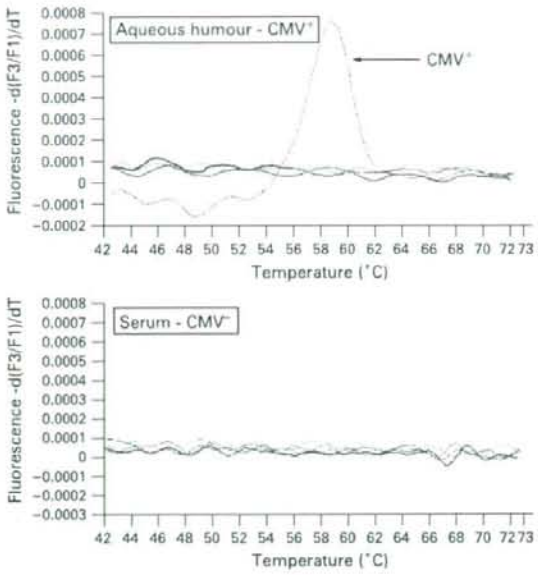

Figure 2 Results for a multiplex PCR in a patient with anterior uveitis. At 58°C, a significant positive curve was seen, indicating the detection of cytomegalovirus (CMV) genomic DNA in the aqueous humour. The other herpes viruses, such as herpes simplex virus (HSV) 1, HSV2, Varicella-zoster virus, Epstein–Barr virus, human herpes virus (HHV6), HHV7 and HHV8, were found to be negative in this particular sample. In addition, CMV-DNA was not detected in the patient's serum.

with several of them reported as being useful in the detection of herpes viruses when various combinations are employed.[7 16 19] In the current study, we were able to rapidly screen for the detection of the virus genome of all eight types of human herpes viruses by using several different primer pairs. When positive results were noted, we then used real-time quantitative PCR to examine the viral load using different primer pairs. This allowed us to confirm our positive results through the use of two PCR combinations.

It is important to discuss the significance of the high viral load of HHV in these patients. The finding of high viral loads in the ocular fluids indicates that virus replication takes place in the eye, suggesting a direct pathogenic role in intraocular inflammation. In the current study, some patients had previously been on systemic or topical corticosteroids over long periods of times before we collected the ocular samples. Therefore, we have to consider that long-term usage of topical and/or systemic steroids might be responsible for the creation of a steroid reservoir that could lead to a localised immunosuppressed state, thereby resulting in HHV replication. In order to be able to avoid the irreversible tissue damage and visual impairment caused by the viral infection, early treatment with anti-viral agents is clinically important, and this can be achieved if there is a rapid and accurate diagnosis of the viral infection in ocular tissues by PCR.

In summary, the HHV family-DNA was detected by multiplex PCR in the ocular fluids of patients with various types of uveitis. Among the positive samples that were identified through the use of qualitative PCR, many of these samples showed significantly high copy numbers of HHV-DNA, when examined by real-time PCR. However, it should be noted that

levels of the viral load for some of the intraocular samples could not be detected, for example, as was seen for the real-time PCR measurement of EBV. Thus, a qualitative multiplex PCR might be a useful method for screening viral infections, and furthermore, quantitative real-time PCR might make it possible to evaluate the clinical relevance of virus infections.

Acknowledgements: We would like to thank S Horie and Y Futagami, for their technical assistance. This work was supported by a Grant-in-Aid for Young Scientists (B) 18791263 of the Ministry of Education, Culture, Sports, Science and Technology, Japan.

Competing interests: None.

Ethics approval: The research followed the tenets of the Declaration of Helsinki, and all study protocols were approved by the Institutional Ethics Committees of Tokyo Medical and Dental University.

Patient consent: Informed consent was obtained from each patient prior to sample collection.

REFERENCES

1. **Ohashi Y,** Yamamoto S, Nishida K, *et al*. Demonstration of herpes simplex virus DNA in idiopathic corneal endotheliopathy. *Am J Ophthalmol* 1991;**112**:419–23.
2. **Yamamoto S,** Tada R, Shimomura Y, *et al*. Detecting varicella-zoster virus DNA in iridocyclitis using polymerase chain reaction. *Arch Ophthalmol* 1995;**113**:1358–9.
3. **Nakamura N,** Tanabe M, Yamada Y, *et al*. Zoster sine herpete with bilateral ocular involvement. *Am J Ophthalmol* 2000;**129**:809–10.
4. **Koizumi N,** Yamasaki K, Kawasaki S, *et al*. Cytomegalovirus in aqueous humor from an eye with corneal endotheliitis. *Am J Ophthalmol* 2006;**141**:564–5.
5. **Arimura E,** Deai T, Maruyama K, *et al*. Herpes simplex virus-2 quantification by real-time polymerase chain reaction in acute retinal necrosis. *Jpn J Ophthalmol* 2005;**49**:64–5.
6. **Asano S,** Yoshikawa T, Kimura H, *et al*. Monitoring herpesvirus DNA in three cases of acute retinal necrosis by real-time PCR. *J Clin Virol* 2004;**29**:206–9.
7. **Chichili GR,** Athmanathan S, Farhatullah S, *et al*. Multiplex polymerase chain reaction for the detection of herpes simplex virus, varicella-zoster virus and cytomegalovirus in ocular specimens. *Curr Eye Res* 2003;**27**:85–90.
8. **Sugita S,** Iwanaga Y, Kawaguchi T, *et al*. Detection of herpesviruses genome by multiplex PCR and real-time PCR in ocular fluids of patients with acute retinal necrosis [in Japanese]. *Nippon Ganka Gakkai Zasshi* 2008;**112**:30–8.
9. **Corey L,** Huang ML, Selke S, *et al*. Differentiation of herpes simplex virus types 1 and 2 in clinical samples by a real-time taqman PCR assay. *J Med Virol* 2005;**76**:350–5.
10. **Kimura H,** Morita M, Yabuta Y, *et al*. Quantitative analysis of Epstein–Barr virus load by using a real-time PCR assay. *J Clin Microbiol* 1999;**37**:132–6.
11. **Gautheret-Dejean A,** Manichanh C, Thien-Ah-Koon F, *et al*. Development of a real-time polymerase chain reaction assay for the diagnosis of human herpesvirus-6 infection and application to bone marrow transplant patients. *J Virol Meth* 2002;**100**:27–35.
12. **Hara S,** Kimura H, Hoshino Y, *et al*. Detection of herpesvirus DNA in the serum of immunocompetent children. *Microbiol Immnol* 2002;**46**:177–80.
13. **Polstra AM,** van den Burg R, Goudsmit J, *et al*. Human herpesvirus 8 load in matched serum and plasma samples of patients with AIDS-associated Kaposi's sarcoma. *J Clin Microbiol* 2003;**41**:5488–91.
14. **Kido S,** Sugita S, Horie S, *et al*. Association of varicella-zoster virus (VZV) load in the aqueous humor with clinical manifestations of anterior uveitis in herpes zoster ophthalmicus and zoster sine herpete. *Br J Ophthalmol* 2008;**92**:505–8.
15. **Takahashi H,** Sugita S, Shimizu N, *et al*. A high viral load of Epstein–Barr virus (EBV) DNA in ocular fluids in a HLA-B27 negative acute anterior uveitis patient with psoriasis. *Jpn J Ophthalmol*. In press.
16. **Kawaguchi T,** Sugita S, Shimizu N, *et al*. Kinetics of aqueous flare, intraocular pressure and virus-DNA copies in a patient with cytomegalovirus iridocyclitis without retinitis. *Inter Ophthalmol* 2007;**27**:383–6.
17. **Sugita S,** Shimizu N, Kawaguchi T, *et al*. Identification of human herpesvirus 6 in a patient with severe unilateral panuveitis. *Arch Ophthalmol* 2007;**125**:1426–7.
18. **Elnifro EM,** Cooper RJ, Klapper PE, *et al*. Multiplex polymerase chain reaction for diagnosis of viral and chlamydial keratoconjunctivitis. *Invest Ophthalmol Vis Sci* 2000;**41**:1818–22.
19. **Druce J,** Catton M, Chibo D, *et al*. Utility of a multiplex PCR assay for detecting herpesvirus DNA in clinical samples. *J Clin Microbiol* 2002;**40**:1728–32.

MAJOR ARTICLE

A New Humanized Mouse Model of Epstein-Barr Virus Infection That Reproduces Persistent Infection, Lymphoproliferative Disorder, and Cell-Mediated and Humoral Immune Responses

Misako Yajima,[1,a] Ken-Ichi Imadome,[1,a] Atsuko Nakagawa,[2] Satoru Watanabe,[3] Kazuo Terashima,[4] Hiroyuki Nakamura,[1] Mamoru Ito,[6] Norio Shimizu,[3] Mitsuo Honda,[5] Naoki Yamamoto,[4,5] and Shigeyoshi Fujiwara[1]

[1]Department of Infectious Diseases, National Research Institute for Child Health and Development, [2]Pathology Laboratory, Department of Clinical Laboratory Medicine, National Center for Child Health and Development, [3]Department of Virology, Division of Medical Science, Medical Research Institute, and [4]Department of Molecular Virology, Graduate School of Medicine, Tokyo Medical and Dental University, and [5]AIDS Research Center, National Institute of Infectious Diseases, Tokyo, and [6]Central Institute for Experimental Animals, Kawasaki, Japan

The functional human immune system, including T, B, and natural killer lymphocytes, is reconstituted in NOD/Shi-*scid*/IL-2Rγ^{null} (NOG) mice that receive hematopoietic stem cell transplants. Here, we show that these humanized mice can recapitulate key aspects of Epstein-Barr virus (EBV) infection in humans. Inoculation with $\sim 1 \times 10^3$ TD_{50} (50% transforming dose) of EBV caused B cell lymphoproliferative disorder, with histopathological findings and latent EBV gene expression remarkably similar to that in immunocompromised patients. Inoculation with a low dose of virus ($\leq 1 \times 10^1$ TD_{50}), in contrast, resulted in apparently asymptomatic persistent infection. Levels of activated $CD8^+$ T cells increased dramatically in the peripheral blood of infected mice, and enzyme-linked immunospot assay and flow cytometry demonstrated an EBV-specific T cell response. Immunoglobulin M antibody specific to the EBV-encoded protein BFRF3 was detected in serum from infected mice. The NOG mouse is the most comprehensive small-animal model of EBV infection described to date and should facilitate studies of the pathogenesis, prevention, and treatment of EBV infection.

Epstein-Barr virus (EBV) is a tumor virus associated with a variety of malignancies, including Burkitt lymphoma, nasopharyngeal carcinoma, and Hodgkin lymphoma [1]. It is also an etiological agent of infectious mononucleosis (IM), which is characterized by transient proliferation of EBV-infected B lymphoblastoid cells and an excessive anti-EBV T cell response. EBV has a unique ability to growth transform human B lymphocytes in vitro and establish lymphoblastoid cell lines (LCLs) [2]. EBV-transformed lymphoblasts express 6 nuclear proteins (Epstein-Barr nuclear antigen [EBNA] 1, 2, 3A, 3B, 3C, and LP) and 3 membrane proteins (latent membrane protein [LMP] 1, 2A, and 2B), and this pattern of EBV gene expression is termed latency III. In contrast, Burkitt lymphoma cells express only EBNA1 consistently (latency I), whereas Hodgkin lymphoma and nasopharyngeal carcinoma cells express EBNA1, LMP1, and LMP2 (latency II). In vivo, EBV-transformed cells are effectively removed by virus-specific cytotoxic T cells, and EBV infection in immunocompetent humans is usually subclinical, except for IM caused by primary infection during adolescence or adulthood. However, in immunocompromised hosts, such as patients with AIDS and transplant recipients, EBV-infected B lymphoblasts can proliferate and cause lymphoproliferative disorder.

Received 28 December 2007; accepted 19 March 2008; electronically published 15 July 2008.

Potential conflicts of interest: none reported.

Financial support: Ministry of Health, Labour, and Welfare of Japan (grants H18-Shinko-013 and H19-AIDS-003).

[a] M.Y. and K.-I. contributed equally to this study.

Reprints or correspondence: Dr. Shigeyoshi Fujiwara, Dept. of Infectious Diseases, National Research Institute for Child Health and Development, 2-10-1 Okura, Setagaya-ku, Tokyo 157-8535, Japan (shige@nch.go.jp); or Dr. Norio Shimizu, Dept. of Virology, Div. of Medical Science, Medical Research Institute, Tokyo Medical and Dental University, 1-5-45 Yushima, Bunkyo-ku, Tokyo 113-8519, Japan (nshivir@tmd.ac.jp); or Dr. Naoki Yamamoto, AIDS Research Center, National Institute of Infectious Diseases, 1-23-1 Toyama, Shinjuku-ku, Tokyo 162-8640, Japan (nyama@nih.go.jp).

The Journal of Infectious Diseases 2008; 198:673–82

0022-1899/2008/19805-0008$15.00

DOI: 10.1086/590502

EBV infects only humans in nature and limited animal species under experimental conditions. It can infect cotton-top tamarins and induce lymphomas, which have been used as a model of EBV-associated lymphomas [3, 4]. Nonhuman primates possess their own lymphocryptoviruses related to EBV, and research on the use of these virus-host systems as models of EBV infection is currently in progress [5, 6]. Small-animal models of EBV have also been developed, which are particularly useful when a large number of animals are necessary. *Scid* mice that receive intraperitoneal transplants of EBV-transformed LCLs or peripheral blood mononuclear cells (PBMCs) isolated from EBV-infected persons develop lymphomas, which have been used as a model of human lymphoproliferative disorder [7–9]. Recently, NOD/*scid* mice transplanted with human hematopoietic stem cells (HSCs) and reconstituted mainly with B lymphocytes were infected with EBV, and the development of lymphoproliferative disorder was described [10]. The immune response to EBV was not studied in these *scid* or NOD/*scid* mouse models. Very recently, a functional human immune system could be reconstituted in highly immunodeficient mouse strains, and these so-called humanized mice were shown able to mount an EBV-specific T cell response [11, 12]. These studies were, however, performed mainly using immunological standpoints and did not provide detailed virological data.

NOD/Shi-*scid*/IL-2Rγ^{null} (referred to here as NOG) is a highly immunodeficient mouse strain that was developed very recently and that, after transplantation with cord blood HSCs, is able to reconstitute most major components of the hematolymphoid system, including T cells, B cells, NK cells, macrophages, and dendritic cells [13–15]. Human T cells that develop in NOG mice are functional in that they can be activated to display cytotoxic activity [15, 16]. These properties made NOG mice an excellent model of human virus infections targeting the immune system, such as those with human T-lymphotropic virus–1 and HIV-1 [17–20]. Here, we provide evidence that humanized NOG mice can reproduce various key aspects of human EBV infection and propose that they may be a valuable tool for studies of EBV infection.

Table 1. Primers for reverse-transcription polymerase chain reaction to detect Epstein-Barr virus (EBV) transcripts.

Transcript, primer	Sequence (5′→3′)
EBNA1	
5′	gatgagcgtttgggagagctgattctgca
3′	tcctcgtccatggttatcac
EBNA2	
5′	agaggaggtggtaagcggttc
3′	tgacgggtttccaagactatcc
LMP1	
5′	ctctcctttctcctcctcttg
3′	caggagggtgatcatcagta
LMP2A	
5′	atgactcatctcaacacata
3′	catgttaggcaaattgcaaa
LMP2B	
5′	cagtgtaatctgcacaaaga
3′	catgttaggcaaattgcaaa
EBER1	
5′	agcacctacgctgccctaga
3′	aaaacatgcggaccaccagc
BZLF1 (first)	
5′	attgcaccttgccgccaccttg
3′	cgcatttttctggaagccacccga
BZLF1 (second)	
5′	gaccaagctaccagagtctat
3′	cagaatcgcattcctccagcga
BMRF1	
5′	ctagccgtcctgtccaagtgc
3′	agccaaacagctccttgccca
BLLF1	
5′	gtcagtacaccatccagagcc
3′	ttggtagacagccttcgtatg
GAPDH	
5′	gcctcctgcaccaccaactg
3′	cgacgcctgcttcaccaccctct

NOTE. EBNA, Epstein-Barr nuclear antigen; EBER, EBV-encoded small RNA; LMP, latent membrane protein.

METHODS

Preparation of humanized mice. NOG mice were obtained from the Central Institute for Experimental Animals (Kawasaki, Japan). Protocols for experiments with NOG mice were approved by the Institutional Animal Care and Use Committee of the National Institute of Infectious Diseases (NIID). Cord blood was supplied by the Tokyo Cord Blood Bank after obtaining informed consent. The use of human materials in this research was approved by the institutional review boards of the National Research Institute for Child Health and Development, the NIID, the Tokyo Medical and Dental University, and the Tokyo Cord Blood Bank. The isolation of human $CD34^+$ HSCs from cord blood by means of the MACS Direct CD34 Progenitor Cell Isolation Kit (Miltenyi Biotec), their intravenous injection (1×10^4 to 1.2×10^5 cells/mouse) into 6–10-week-old female NOG mice, and the characterization of the reconstitution of the human hematoimmune system were done as described elsewhere [18, 20]. NOG mice in which the human hematoimmune system was reconstituted are referred here as humanized NOG (hNOG) mice.

Experimental EBV infection, quantification of viral DNA, and detection of viral mRNAs. Virus production by EBV-infected Akata cells was stimulated by brief treatment with anti-IgG antibody (Dako), and culture fluid was used as inoculum after filtration through a 0.45-μm membrane filter [21]. For virus titration, cord blood lymphocytes were plated at the density